Article

Cell

Multi-organ Mapping of Cancer Risk

Graphical Abstract

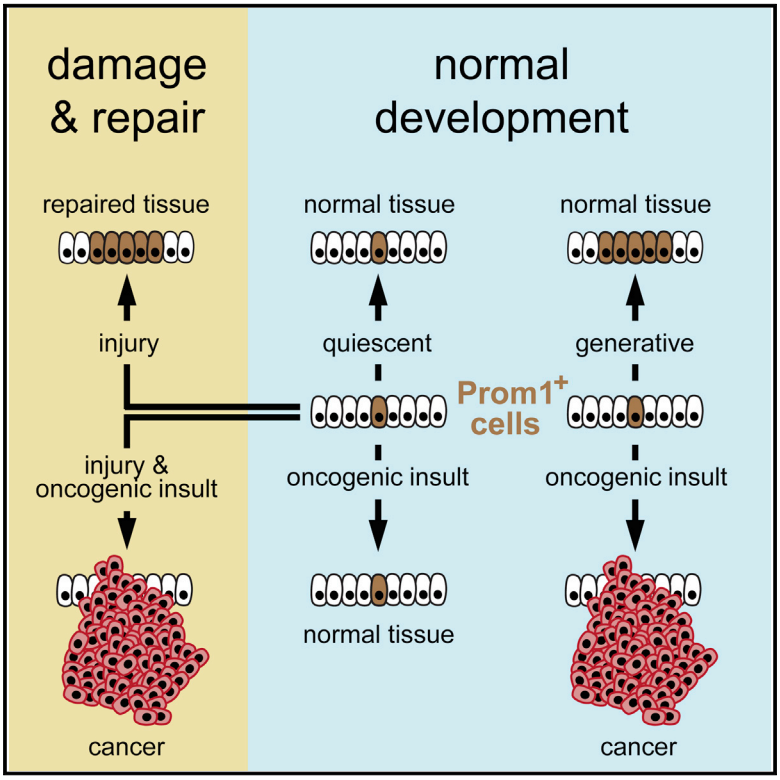

Authors

Liqin Zhu, David Finkelstein, Culian Gao, ..., David Ellison, Arzu Onar-Thomas, Richard James Gilbertson

Correspondence

arzu.onar@stjude.org (A.O.-T.), richard.gilbertson@cruk.cam.ac.uk (R.J.G.)

In Brief

The generative capacity of an organ's stem cells determines the life-long risk for developing cancer in that organ.

Highlights

- Prom1$^+$ cells display different generative and tumorigenic capacities among organs
- Prom1$^+$ cell transformation is determined by life-long generative capacity
- Prom1 marks neonatal liver and damage-induced adult liver stem cells
- Stem cell gene expression patterns predict oncogenes and tumor suppressors

Data Resources

GSE78076

Zhu et al., 2016, Cell *166*, 1132–1146
August 25, 2016
http://dx.doi.org/10.1016/j.cell.2016.07.045

CellPress

Multi-organ Mapping of Cancer Risk

Liqin Zhu,[1] David Finkelstein,[2] Culian Gao,[3] Lei Shi,[3] Yongdong Wang,[2] Dolores López-Terrada,[4] Kasper Wang,[5] Sarah Utley,[5] Stanley Pounds,[3] Geoffrey Neale,[6] David Ellison,[7] Arzu Onar-Thomas,[3,*] and Richard James Gilbertson[8,9,*]
[1]Department of Developmental Neurobiology
[2]Department of Computational Biology
[3]Department of Biostatistics
St. Jude Children's Research Hospital, 262 Danny Thomas Place, Memphis, TN 38105, USA
[4]Department of Pathology & Immunology, Baylor College of Medicine, 1 Baylor Plaza, Houston, TX 77030, USA
[5]Developmental Biology, Regenerative Medicine, and Stem Cell, Division of Pediatric Surgery, Children's Hospital Los Angeles, 4650 Sunset Boulevard, Los Angeles, CA 90027, USA
[6]Hartwell Center
[7]Department of Pathology
St. Jude Children's Research Hospital, Memphis, TN 38105, USA
[8]Department of Oncology and CRUK Cambridge Institute, Robinson Way, Cambridge CB2 0RE, England
[9]Lead Contact
*Correspondence: arzu.onar@stjude.org (A.O.-T.), richard.gilbertson@cruk.cam.ac.uk (R.J.G.)
http://dx.doi.org/10.1016/j.cell.2016.07.045

SUMMARY

Cancers are distributed unevenly across the body, but the importance of cell intrinsic factors such as stem cell function in determining organ cancer risk is unknown. Therefore, we used Cre-recombination of conditional lineage tracing, oncogene, and tumor suppressor alleles to define populations of stem and non-stem cells in mouse organs and test their life-long susceptibility to tumorigenesis. We show that tumor incidence is determined by the life-long generative capacity of mutated cells. This relationship held true in the presence of multiple genotypes and regardless of developmental stage, strongly supporting the notion that stem cells dictate organ cancer risk. Using the liver as a model system, we further show that damage-induced activation of stem cell function markedly increases cancer risk. Therefore, we propose that a combination of stem cell mutagenesis and extrinsic factors that enhance the proliferation of these cell populations, creates a "perfect storm" that ultimately determines organ cancer risk.

INTRODUCTION

Cancers are distributed unevenly across the body. Some organs are far more likely to undergo malignant change than others, and children and adults develop very different types of cancer (Howlader et al., 2012). This temporal and topographical bias in cancer formation can be explained in part by organ-specific susceptibilities to carcinogens or inherited oncogenic mutations; but the relative contributions of these, or other factors, to organ cancer risk is unknown (Danaei et al., 2005; Futreal et al., 2004). A greater understanding of the processes that underlie tumorigenesis is crucial if we are to improve the prevention and treatment of cancer.

It was recently proposed that the number of stem cell divisions occurring in a tissue during life might dictate cancer risk (Tomasetti and Vogelstein, 2015). This so-called "bad luck" hypothesis states that many cancers arise following the propagation of mutations that occur by chance in highly-replicative stem cell populations, rather than following exposure to environmental carcinogens. An important implication of this hypothesis is that these cancers are unavoidable and therefore resistant to primary prevention. But the notion that "intrinsic" factors such as stem cell replication are more important than "extrinsic" factors in carcinogenesis has been strongly contested (Ashford et al., 2015; Gotay et al., 2015; O'Callaghan, 2015; Potter and Prentice, 2015; Song and Giovannucci, 2015; Wild et al., 2015; Wu et al., 2016). Indeed, recent mathematical modeling estimated that 70%–90% of the causal factors driving the most common cancers are "extrinsic" (Wu et al., 2016).

The controversy surrounding these studies of cancer risk stems largely from their use of different mathematical approaches to correlate selected human cancer incidence data with variable sources and types of stem cell proliferation metrics. While these studies are important, they do not allow direct testing of the relationship between "intrinsic" factors such as stem cell proliferation and cancer risk and cannot account adequately for "extrinsic" carcinogenic factors. Experiments testing these variables directly could provide crucial insights into cancer origins but they have not been performed on an adequate scale, in appropriate experimental systems. Therefore, we performed a series of organism-wide linage tracing and tumorigenesis studies, in defined populations of cells, in neonatal and adult mice, to more directly identify cell properties that dictate organ cancer risk.

RESULTS

Prom1$^+$ Cell Generative Capacity Varies among Organs and Developmental Stages

As a first step to test the relationship between cell properties and cancer risk, we characterized the number, basal proliferation

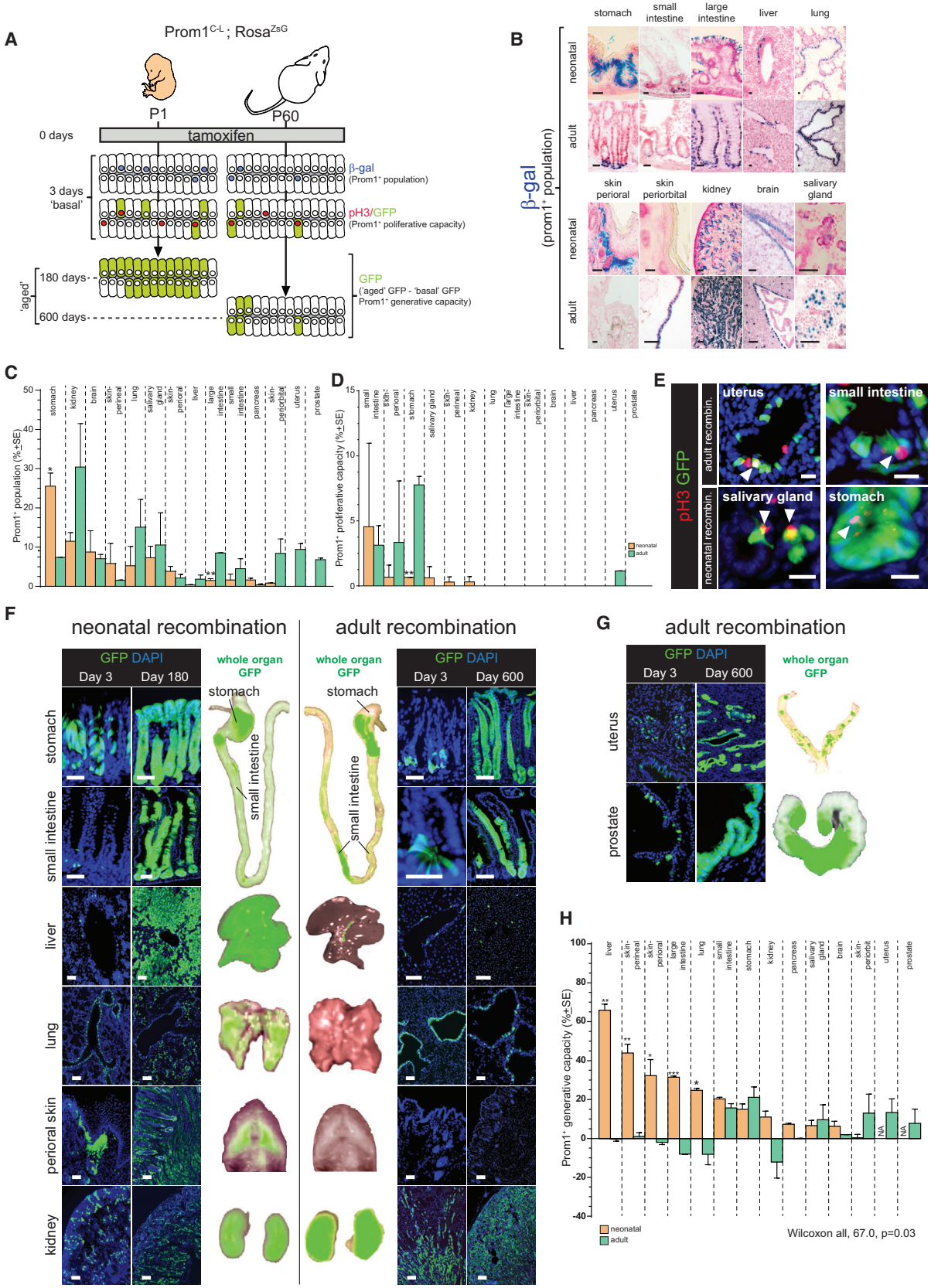

(legend on next page)

rate, and life-long generative capacity of defined cell populations across major organs in neonatal (postnatal day [P]1) and adult (P60) mice. To do this we used our *Prom1*$^{C-L}$ mouse that expresses both CreER2-recombinase and LacZ from the endogenous *Prom1* (*Cd133*) locus (Zhu et al., 2009). We focused on Prom1$^+$ cells because Prom1 marks a variety of cell types in mouse organs (Zhu et al., 2009), as well as some normal and malignant human stem cells (Lee et al., 2005; O'Brien et al., 2007; Ricci-Vitiani et al., 2007; Singh et al., 2004; Yin et al., 1997). First, a *Rosa-ZsGreen Fluorescence Protein* lineage tracing allele (*Rosa*^{ZsG}) was activated by tamoxifen-induced recombination in neonatal (n = 20) and adult (n = 20) *Prom1*$^{C-L}$; *Rosa*^{ZsG} mice. Three days later, organs were collected from ten mice each in both age groups ("basal" organs; Figure 1A). The remaining mice were allowed to age for 180 days (neonatal-induced) or 600 days (adult-induced) and their organs were then collected ("aged" organs). Bone marrow and peripheral blood samples were also taken for GFP fluorescence-activated cell sorting (FACS) of hematopoietic lineages.

β-galactosidase and GFP staining detected similar numbers and distributions of Prom1$^+$ cells in "basal" organs, indicating *Prom1*$^{C-L}$ drives efficient recombination across all major organs (Figures 1B and 1F and data not shown). The size of the Prom1$^+$ cell population varied markedly among "basal" organs, ranging from the greatest in adult kidney (30.4% ± 13.3% SE) to the smallest in neonatal liver (0.4% ± 0.04% SE; Figures 1B, 1C, 1F, and 1G); however, within any given organ, the number and location of Prom1$^+$ cells remained fairly constant between neonates and adults. We then quantified Prom1$^+$ cell proliferative capacity by co-immunostaining "basal" organs with GFP and the cell proliferation marker pH3. Only limited Prom1$^+$ proliferative capacity was detected in a handful of organs at both ages (Figures 1D and 1E).

To determine which organs might contain Prom1$^+$ stem cells, we calculated the generative capacity of Prom1$^+$ cells by measuring the difference in the proportion of GFP$^+$ cells in lineage-traced "aged" organs with those in the corresponding "basal" organ (Figure 1A). In select organs with high generative capacity, we also fate-mapped Prom1$^+$ cell progeny to see if these included differentiated cells. In this manner, we showed previously that adult small intestinal Prom1$^+$ stem cells generate the entire intestinal mucosa (Zhu et al., 2009). Although the number and location of Prom1$^+$ cells in each organ remained fairly constant between neonates and adults, those in neonates frequently displayed a greater generative capacity (Figure 1H; across all organs, $p < 0.05$, Wilcoxon). For example, Prom1$^+$ cells in both neonatal and adult livers were sparse and located within or adjacent to the Krt19$^+$ bile duct epithelium; a proportion of these cells co-expressed the liver progenitor marker A6 (Figures 1B, 1C, 1F, S1A, and S1B). However, while Prom1$^+$ cells in neonatal livers were highly generative and produced the majority of ductal cells and hepatocytes that populated the liver by P180; those in adults had no detectable generative capacity ($p < 0.005$ Mann-Whitney; Figures 1B, 1F, 1H, and S1B). Other organs in which Prom1$^+$ cell generative capacity was restricted to neonates included the perineal skin ($p < 0.005$), perioral skin ($p < 0.05$), large intestine ($p < 0.0005$), and lung ($p < 0.05$; Figures 1F and 1H).

In other organs, both adult and neonatal Prom1$^+$ cells displayed similar generative capacities. Prom1$^+$ cells were localized to the base of gastric pits in both neonates and adults—the same location as adult Lgr5$^+$ gastric stem cells (Barker et al., 2010)—and produced mature pit (UEAI$^+$), neck (GSII$^+$), and parietal (DBA$^+$) cells of the gastric epithelium (Figures 1B, 1F, 1H, and S2A). Prom1$^+$ cells in the crypts of neonatal and adult small intestines also displayed similar generative capacities and produced all mature cell types of the intestinal mucosa. In contrast, Prom1$^+$ cells in both neonatal and adult kidney, pancreas, salivary gland, and brain displayed limited or no generative capacity (Figure 1H). Similarly, no GFP$^+$ cells were detected in the bone marrow or blood of "aged" mice (data not shown). These data are in agreement with recent reports that mouse hematopoietic stem cells cannot be isolated on the basis of Prom1 expression (Arndt et al., 2013).

Tamoxifen treatment caused involution of the neonatal prostate and uterus, precluding accurate lineage-tracing of Prom1$^+$ cells in these organs. However, serial rounds of androgen deprivation and replacement in castrated adult male mice caused Prom1$^+$ cells to regenerate the entire prostatic mucosa, including basal (p63$^+$) and luminal (Androgen Receptor$^+$) cells, while serial estrous cycles induced Prom1$^+$ cells to regenerate the uterine mucosa (Figures 1G, 1H, and S2A–S2C; STAR Methods).

As a further test of the stem cell nature of Prom1$^+$ cells we used Gene Set Enrichment Analysis to compare the transcriptomes of Prom1$^+$ cells (>98% purity) isolated from various adult organs as well as neonatal livers (sufficient pure Prom1$^+$ cell isolates could not be obtained from other neonatal organs) with those of 67 published stem cell gene expression signatures. A significant and positive correlation was observed between the generative capacity of Prom1$^+$ cells and their enrichment of stem cell signatures ($R^2 = 0.80$, $p < 0.005$; Figure S3; Table S1). Thus, our data reveal marked variation in the generative capacity associated with Prom1$^+$ cells among organs and provide strong evidence that Prom1$^+$ cells in the adult small intestine, stomach, prostate, and uterus, and the neonatal liver are stem cells.

Figure 1. Prom1$^+$ Cell Properties in Major Organs of *Prom1*$^{C-L}$; *Rosa*^{ZsG} Mice

(A) Overall approach used the measure Prom1$^+$ cell number, proliferative, and generative capacities across organs of neonatal and adult mice.

(B) β-galactosidase staining of Prom1$^+$ cells in neonatal and adult *Prom1*$^{C-L}$ mouse tissues. Scale bars, 10 μm (top panels); 50 μm (bottom panels).

(C and D) Percentage of Prom1$^+$ cells (C) and percentage of proliferating Prom1$^+$ cells (D) in indicated tissues. Data in (C) and (D) represent mean ± SE.

(E) Arrows identify proliferating Prom1$^+$ cells in indicated tissues 1 day post tamoxifen. Scale bars, 10 μm.

(F and G) Direct GFP fluorescence microscopy of tissues at the indicated times post tamoxifen treatment. Whole organ direct GFP fluorescence images are also shown. Scale bars, 50 μm.

(H) Prom1$^+$ cell-generative capacity in indicated tissues. *$p < 0.05$; **$p < 0.005$; ***$p < 0.0005$. Data represent mean ± SE.

See also Figures S1, S2, and S3 and Table S1.

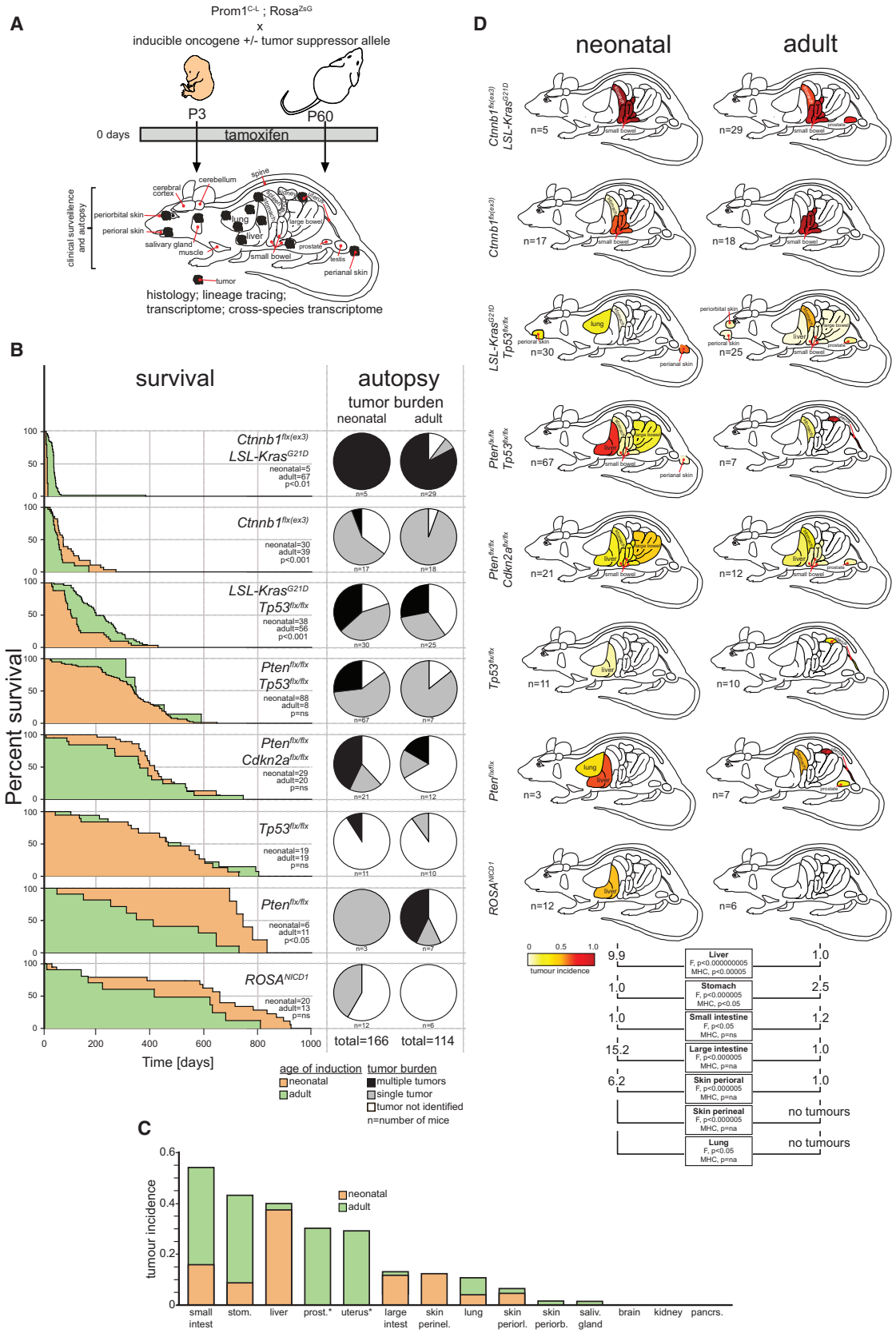

(legend on next page)

Prom1^{+} Cell Susceptibility to Transformation Varies among Organs and Developmental Stages

Having characterized the number, basal proliferation, and generative capacity of Prom1^{+} cells in neonatal and adult organs, we next tested the susceptibility of these cells to tumorigenesis (Figure 2A). We reasoned that different tissues might be sensitive to different initiating oncogenes and tumor suppressor genes (TSGs). To characterize this variability in susceptibility, we selected a broad range of conditional alleles that disrupt major signaling pathways perturbed in human cancer, including *Ctnnb1*$^{flx(ex3)}$, *Kras*^{G12D}, *Rosa*^{NICD1}, *Tp53*$^{flx/flx}$, *Pten*$^{flx/flx}$, and *Cdkn2a*$^{flx/flx}$ (Futreal et al., 2004). Mice carrying these alleles were bred with *Prom1*$^{C\text{-}L}$; *Rosa*^{ZsG} mice to generate a total of eight mouse lines each harboring these conditional alleles either alone or in combination (Figure 2B). To parallel our lineage tracing study, oncogene and TSG conditional alleles were recombined by tamoxifen treatment of neonatal (P1) and adult (P60) mice. A total of 468 mice (n = 235 neonates and 233 adults) across the eight genotypes were recombined and subjected to life-long tumor surveillance studies (Table S2). Median survival rates varied greatly among the different genotypes, ranging from 11 days post-tamoxifen survival in neonatal-induced *Prom1*$^{C\text{-}L}$; *Rosa*^{ZsG}; *Ctnnb1*$^{flx(ex3)}$; *Kras*^{G12D} mice, to 743 days post-tamoxifen survival in neonatal-induced *Prom1*$^{C\text{-}L}$; *Rosa*^{ZsG}; *Pten*$^{flx/flx}$ mice (Figure 2B). Significant differences in survival were also observed between neonatal and adult-induced mice of the same genotype (Figure 2B).

To determine if the recombination of oncogene and TSG alleles in Prom1^{+} cells induced cancer, we performed full autopsies on 166 neonatal-induced and 114 adult-induced mice that became moribund (Figures 2B–2D; Table S2). Organs from all animals were inspected both macro- and microscopically for evidence of tumor formation. A total of 316 tumors were identified across the 280 autopsies. A single tumor was identified in 46% (n = 76/166) and 33% (n = 38/114) of neonatal and adult-induced mice, respectively. A further 28% (n = 46/166) of neonatal-induced and 30% (n = 34/114) of adult-induced mice contained multiple tumors (range, two to five distinct primaries; Table S2). Ninety-seven percent (n = 307/316) and 3% (n = 9/316) of all tumors were judged to be primary or metastatic, respectively, by the reviewing pathologists (Figure 3A; Table S2). All primary and secondary tumors were GFP^{+} (Figure 3A). Primary tumors included small and large intestinal adenomas, stomach adenomas and adenocarcinomas, hepatocellular carcinomas/intrahepatic cholangiocarcinomas (HCC/ICC), hepatoblastomas, prostatic adenocarcinomas, uterine carcinomas, squamous cell skin cancers, and lung adenomas (Figures 2B–2D and 3A; Table S2). Few or no tumors and no premalignant lesions were found in the salivary gland, kidney, brain, or pancreas even though some of these had large populations of Prom1^{+} cells and would therefore have received a significant mutational burden. A total of 204 genotype-matched mice were also aged without tamoxifen induction to assess rates of spontaneous tumor formation. Only 2.5% (n = 5/204) of these mice developed tumors that were all GFP^{-} (Table S2). Thus, tumors in our model systems arose within recombined Prom1^{+} cell lineages.

Because almost one-third of mice developed multiple tumors, of which some appeared to be metastatic, we sought to more rigorously assess the accuracy of our histological diagnoses. To do this, we subjected 58 primary and 7 metastatic tumors to gene expression profiling (Figure 3B; Table S3; GEO78076). Unsupervised hierarchical clustering segregated out liver, skin, carcinomas, and adenomas. Within these clusters, tumors of the same histological type, including metastatic tumors harvested from distal sites, were co-clustered. As a further test of histologic tumor typing, we used our cross-species AGDEX algorithm (Johnson et al., 2010) to compare the transcriptomes of our mouse tumors with those of 154 histologically matched human primary cancers (Table S4). The transcriptomes of mouse HCC/ICC, skin squamous cell, prostate, and uterine carcinomas, and colonic adenomas closely matched those of the corresponding human tumor (Figure 3C). Thus, Prom1^{+} cell populations in some, but not all, mouse organs are susceptible to transformation and generate cancers that recapitulate the histology and transcriptome of the corresponding human tumors.

Prom1^{+} Cell Transformation Is Partly Determined by Initiating Mutation

Organ bias in tumor formation in our mice could be explained in part by tissue-specific susceptibilities to initiating mutations. For example, in keeping with the high rate of WNT pathway mutations in human intestinal tumors (Bienz and Clevers, 2000), 73% (n = 16/22) of neonatal and 91% (n = 43/47) of adult-induced mice harboring the *Ctnnb1*$^{flx(ex3)}$ allele developed small intestinal adenomas, compared with only 13% of neonatal (n = 12/144) and 3% (n = 2/67) of adult-induced mice that lacked the allele (Figures 2B–2D and 3A; Table S2; Fisher's exact, $p < 0.00001$). Additionally, consistent with the high rate of *PTEN* mutations in human uterine cancer (Kong et al., 1997; Risinger et al., 1997), 89% (n = 8/9) of female adult-induced mice carrying the *Pten*$^{flx/flx}$ allele developed uterine carcinomas versus only 5% (n = 1/22) of adult-induced females with wild-type *Pten* (Fisher's exact, $p < 0.0001$). Different initiating mutations also induced different types of tumors within the same organ. For example, 100% (n = 5/5) of liver tumors in neonatal-induced *Prom1*$^{C\text{-}L}$; *Rosa*^{ZsG}; *Rosa*^{NICD1} mice were Ctnnb1^{+}/Hes1^{+}/GS^{+}/Sall4^{+} hepatoblastomas, while 100% (n = 64/64) of liver tumors arising in the other genotypes were HCC/ICC (Figure 3A; Table S2; Fisher's

Figure 2. Prom1^{+} Cell Susceptibility to Tumorigenesis in Major Organs of *Prom1*$^{C\text{-}L}$; *Rosa*^{ZsG} Mice

(A) Overall approach used to measure Prom1^{+} cell susceptibility to tumorigenesis.

(B) Left: survival curves of neonatal and adult *Prom1*$^{C\text{-}L}$; *Rosa*^{ZsG} mice carrying the indicated alleles. p value = difference in adult and neonatal survival. Right: pie charts of numbers of mice autopsied containing no, single or multiple tumors.

(C) Incidence of tumors in the indicated tissues across all genotypes.

(D) Anatomical heatmaps of organ tumor incidence. Below, ratios of tumors in neonatal and adult tissues. F, Fisher's test of the difference; CMH, Cochran-Mantel-Haenszel test of the difference.

See also Table S2.

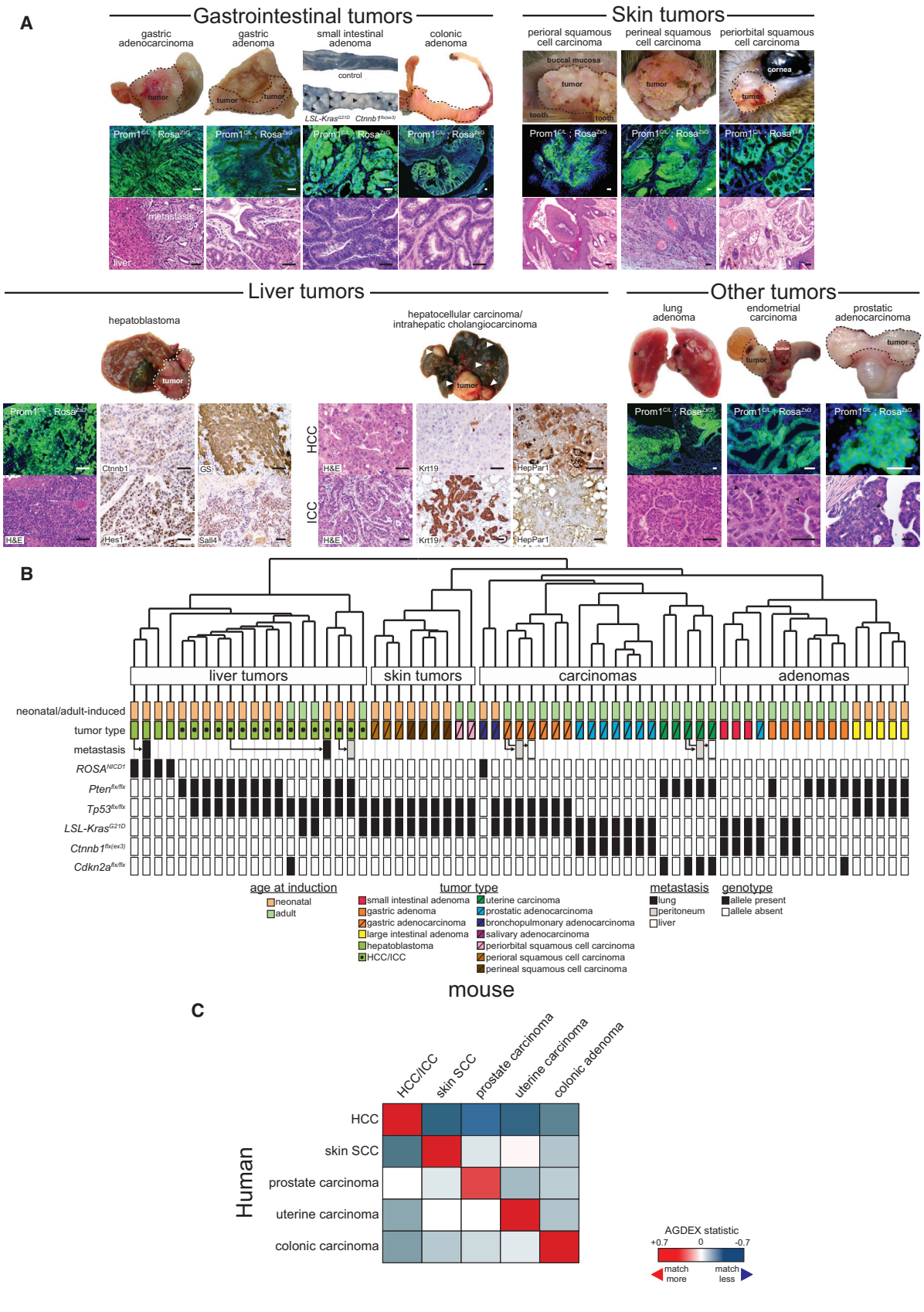

(legend on next page)

exact, $p < 0.00005$). Similarly in the stomach, all tumors arising in *Prom1*$^{C\text{-}L}$; *Rosa*^{ZsG}; *Kras*^{G12D}; *Tp53*$^{flx/flx}$ mice (n = 12/12) and *Prom1*$^{C\text{-}L}$; *Rosa*^{ZsG}; *Pten*$^{flx/flx}$; *Tp53*$^{flx/flx}$ mice (n = 5/5) were gastric adenocarcinomas, while all 37 stomach tumors arising in the other five affected genotypes were gastric adenomas; suggesting loss of *Tp53* might be an important determinant of carcinoma formation in the stomach (Figure 3A; Table S2; Fisher's exact, $p < 0.00005$).

However, initiating mutations did not fully explain the temporal and topographical bias in tumorigenesis among organs. For example, the liver, small intestine, and stomach appeared to show an age-specific bias in tumor development in the context of multiple genotypes. Therefore, we used the Cochran-Mantel-Haenszel test to determine if developmental stage and tumor prevalence in these organs were associated even when multiple genotypes were oncogenic. These analyses showed that neonatal-induced mice had a 10-fold average greater incidence of liver tumors than adult-induced mice, which was consistent across genotypes (common odds ratio [COR] P3:P60 = 9.9; Cochran-Mantel-Haenszel test [CMH], $p < 0.0005$; Figures 2C and 2D). Also consistent across genotypes, significantly more stomach tumors arose in adult than neonatal-induced mice (COR P60:P3 = 2.5, CMH, $p < 0.05$). Furthermore, even those organs that were susceptible to specific initiating mutations demonstrated a temporal bias in cancer formation, including small intestinal adenomas associated with *Ctnnb1* activation that were more common in adult-induced mice (Figure 2D; Fisher's exact, $p < 0.05$), *Pten*-deleted large intestinal and lung adenomas, both of which were more common in neonatal-induced mice (Fisher's exact, $p < 0.05$), and perioral and perineal squamous cell carcinomas in *Kras*-activated/*Tp53*-deleted mice that were more common in neonatal-induced mice (Fisher's exact, $p < 0.000005$). Thus, Prom1$^+$ cell populations in some organs were differentially susceptible to transformation independent of initiating mutation, suggesting that other cell properties might have dictated patterns of cancer development in our mice.

Prom1$^+$ Cell Generative Capacity Is a Major Determinant of Organ Cancer Risk

To begin to understand what cell properties might dictate cancer risk, we used mathematical modeling to explore how Prom1$^+$ cell population size, proliferative capacity, and generative capacity in each organ related to susceptibility to tumorigenesis. All tumorigenesis and Prom1$^+$ cell data from all organs in neonatal and adult-induced mice were incorporated into a generalized linear mixed model with a logit link (GLMM-LL) to assess these relationships because this allowed incorporating multiple tumors within mice, genotype to be treated as a random effect, and mice to be nested within genotype (McCulloch et al., 2008).

In single marker models that incorporated an interaction with age, Prom1$^+$ generative capacity provided the most robust model: the greater the generative capacity of a Prom1$^+$ cell in an organ, the more susceptible it was to tumorigenesis, strongly suggesting that Prom1$^+$ stem cells are especially tumorigenic (Figure 4A; note the smaller the Akaike Information Criterion [AIC] the better the model fit). This notion is further supported by the observation that organs containing the smallest populations of Prom1$^+$ cells were most likely to generate tumors, because stem cells are relatively rare in tissues (Figure 4A; AIC = 2,255). Interestingly, neonatal and adult Prom1$^+$ cells with equivalent generative capacities displayed markedly different susceptibilities to transformation: those in neonates were significantly more resistant to tumorigenesis ($p = 5 \times 10^{-11}$). Prom1$^+$ proliferative capacity also increased cancer risk, although less dramatically than generative capacity (Figure 4B; AIC = 2,138).

Because Prom1$^+$ population size, proliferative capacity, and generative capacity may be interrelated, we used GLMM-LL iterative multivariable modeling to determine the relative association of these factors with cancer risk (Figures 4D and 4E). Once again, Prom1$^+$ generative capacity was most significantly and positively correlated with tumor incidence (both induction ages, $p < 2 \times 10^{-16}$). Prom1$^+$ proliferative capacity was also related to cancer risk in neonatal-induced mice, but only marginally so in adult-induced mice. Prom1$^+$ population size was not related independently to tumor incidence. Thus, our data strongly suggest that the risk of an organ developing cancer following the introduction of oncogenic mutations into its resident Prom1$^+$ cell population is significantly associated with their life-long generative capacity: this holds true in the presence of multiple genotypes and regardless of developmental stage, supporting the notion that the mutation of stem cells dictates cancer risk.

Hepatic Tumorigenesis Varies Directly with Prom1$^+$ Cell Generative Capacity

To further explore the notion that stem cell phenotype dictates cancer risk, we looked to see if altering stem cell properties in a single organ might concurrently alter tumorigenesis. Similarly sized and located populations of Prom1$^+$ cells exist in neonatal and adult livers but only those in neonates are generative and tumorigenic (Figures 1, 2, 3, and S1). Therefore, we hypothesized that adult Prom1$^+$ liver cells might be the quiescent progeny of neonatal Prom1$^+$ liver cells. To test this, we fate mapped Prom1$^+$ liver cells in neonatal *Prom1*$^{C\text{-}L}$; *Rosa*^{ZsG} mice and demonstrated that these cells, or their progeny, constitute 94.6% + 0.3% SD of Prom1$^+$ cells in adult liver (Figure 5A).

Chronic tissue injury plays a critical role in tumorigenesis, particularly in the liver where cancer is rare in the absence of chronic tissue damage (Block et al., 2003; Coussens and Werb, 2002; Pikarsky et al., 2004). Therefore, we next tested if

Figure 3. Histology and Transcriptomic Analysis of Prom1$^+$ Cell-Derived Tumors in Mice

(A) Top: gross specimens (arrows and dotted lines denote tumors), and photomicrographs of direct GFP fluorescence, liver immunohistochemistry (HCC and hepatoblastoma marker expression), and H&E stains (arrows denote mitoses) of exemplary tumors. Scale bars, 50 μm.

(B) Unsupervised hierarchical clustering of mouse tumors. Details of age at recombination, tumor histology, and genotype are shown below.

(C) AGDEX comparison of histologically matched human and mouse tumors.

See also Tables S3 and S4.

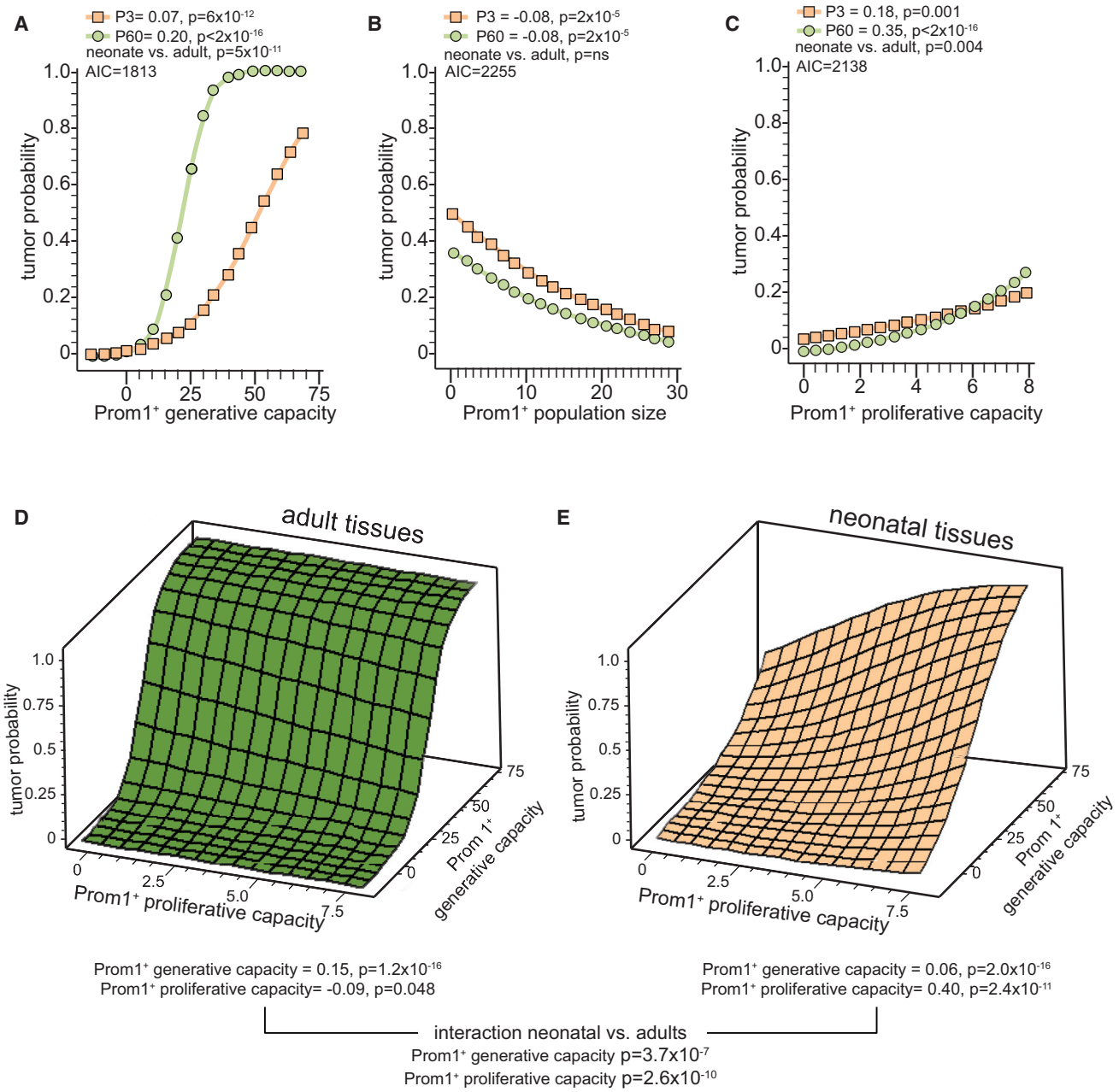

Figure 4. Relationship of Prom1$^+$ Cell Characteristics to Tumor Susceptibility

(A–C) Generalized linear mixed models with a logit link (GLMM-LL) of tumor probability versus Prom1$^+$ cell generative capacity (A), Prom1$^+$ cell population size (B), and Prom1$^+$ cell proliferative capacity (C). Numbers at top of each graph indicate the regression coefficients and p value of each as well as the Akaike Information Criterion score.

(D and E) GLMM-LL iterative multivariable modeling of tumor probability versus Prom1$^+$ cell generative and proliferative capacities in adult (D) and neonatal (E) tissues.

See also STAR Methods.

damaging adult livers might reactivate generative and tumorigenic capacity in Prom1$^+$ adult liver cells. Lineage tracing alleles were activated in adult *Prom1*$^{C\text{-}L}$ mice by tamoxifen-recombination and then 3 days later their livers were damaged by either partial hepatectomy (Michalopoulos and DeFrances, 1997) or administration of diethoxycarbonyl-1,4-dihydrocollidine (DDC) (Preisegger et al., 1999). Both damage mechanisms markedly activated Prom1$^+$ cell proliferation and tissue repair (Figures 5B and S1B). Remarkably, AGDEX and GSEA analyses revealed that while the transcriptomes of Prom1$^+$ cells isolated from

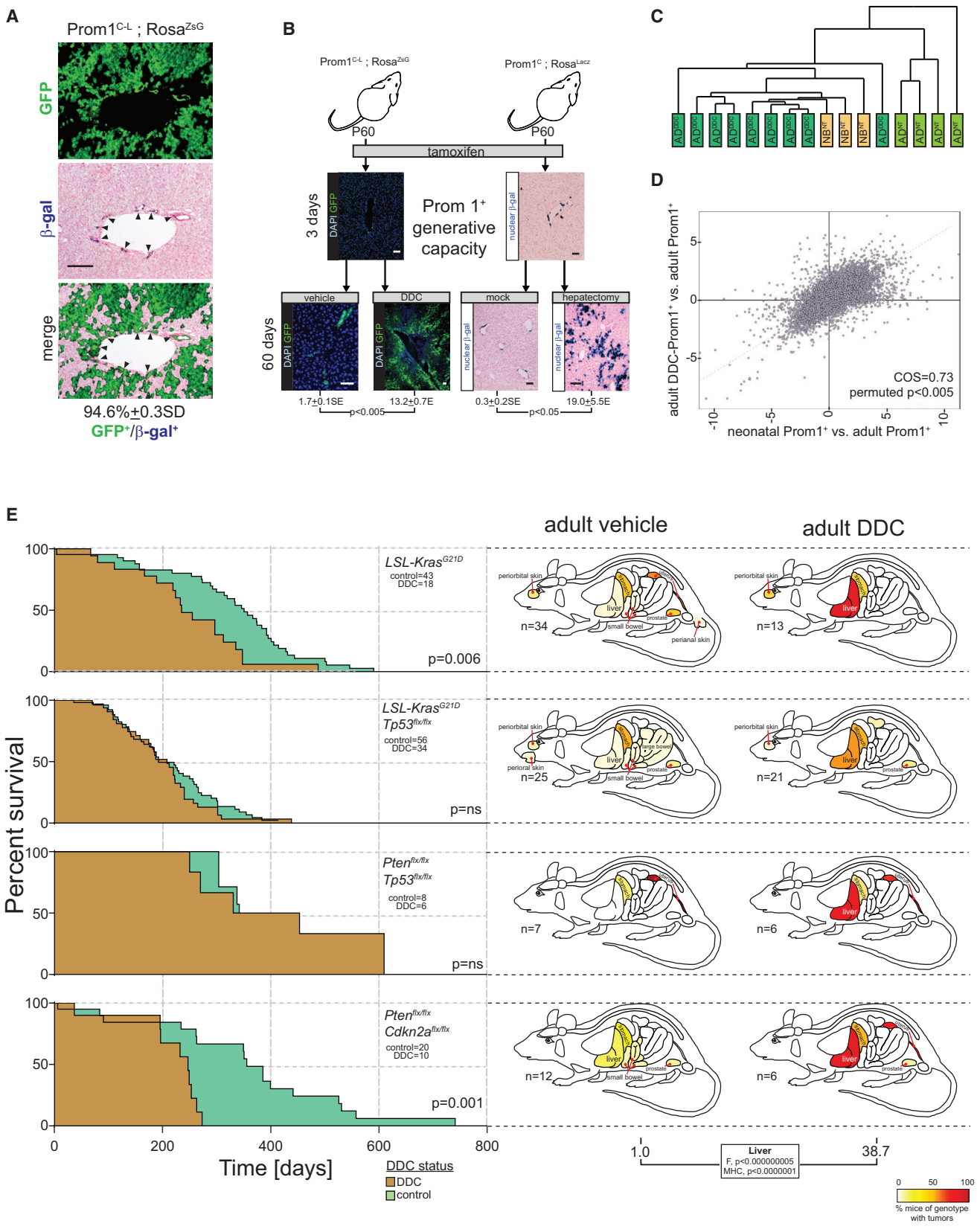

(legend on next page)

damaged adult livers did not resemble those of normal adult liver, they were very similar to those of neonatal Prom1^{+} liver cells and were enriched with many of the "stem cell signatures" observed in neonatal Prom1^{+} liver cells (Figures 5C and 5D; Table S1). Thus, adult Prom1^{+} liver cells are the quiescent progeny of neonatal Prom1^{+} liver stem cells: damaging the liver reactivates a "neonatal-like" stem cell program in these cells, promoting their proliferation and liver repair. Because damaged adult liver Prom1^{+} cells did not upregulate Lgr5 (Figure S1C), they are likely to be distinct from Lgr5^{+} damage-induced hepatocytes (Huch et al., 2013).

To test if damage-induced generative capacity of adult Prom1^{+} liver cell increases their susceptibility to tumorigenesis, we repeated our sequential Cre-recombination and DDC-damage protocol in *Prom1*$^{C\text{-}L}$;*Rosa*^{ZsG} mice harboring *Kras*^{G12D}, *Kras*^{G12D}; *Tp53*$^{flx/flx}$, *Pten*$^{flx/flx}$; *Tp53*$^{flx/flx}$, or *Pten*$^{flx/flx}$; *Cdkn2a*$^{flx/flx}$ alleles (n = 68). All mice were subjected to tumor surveillance for at least 2 years and moribund mice underwent full autopsies (DDC-treated, n = 46; control, n = 78; Figure 5E; Table S2). Liver damage dramatically increased the production of liver tumors by mutated Prom1^{+} cells across all genotypes (COR, DDC:control = 38.7, CMH, $p < 1 \times 10^{-7}$; Figure 5E). Although DDC was delivered systemically, the incidence of other cancers remained unchanged; indicating that acceleration of tumorigenesis by DDC was specific to the liver (Table S2). Indeed, consistent rates of tumorigenesis in other organs likely explained why the survival of DDC and non-DDC mice remained relatively similar for most genotypes. For example, non-DDC- and DDC-treated *Kras*^{G12D}; *Tp53*$^{flx/flx}$ mice succumbed to aggressive gastric adenocarcinomas with similar median survivals (non-DDC = 209 days; DDC = 193 days), even though all DDC-treated animals developed liver tumors. Thus, the reactivation of generative capacity in adult Prom1^{+} liver cells markedly increases their susceptibility to transformation, providing direct evidence that cell generative capacity can be a major determinant of organ cancer risk.

Cross-Species Analysis Predicts the Role of Recurrently Mutated Genes in Human Cancer

Because Prom1^{+} stem cells were peculiarly susceptible to transformation, we speculated that gene expression patterns in these cells might inform understanding of cancer, and in particular, unmask the role of genes that are recurrently mutated in cancer.

To test this, we first identified 657 genes that The Cancer Genome Atlas reported as recurrently mutated (n > 3 samples) in human hepatocellular, gastric, prostatic, or uterine carcinomas (http://www.cbioportal.org). We studied these cancers because the corresponding tumors in our mice arose from Prom1^{+} stem cells. Only 18% of the 657 mutated genes are validated as either oncogenes (n = 58/657) or TSGs (n = 60/657); the function in cancer of the remaining 82% (n = 539/657) is unknown. Next, we identified the cancers in which each gene was most and least frequently mutated, reasoning that these tissues were most and least likely to be transformed by mutations in the gene (Figure 6A). We then compared the log ratio of expression of each of these genes in Prom1^{+} versus Prom1^{-} cells of the corresponding tissues in mice (hereon, Prom1^{+} log ratio difference [LRD]). Almost twice as many validated oncogenes (n = 42/66) than TSGs (n = 24/66) had a positive LRD, while more than twice as many TSGs (n = 36/52) than oncogenes had a negative LRD (n = 16/52; $p < 0.0005$; Figure 6B). Even greater bias was observed among genes with an LRD >3 and <−3, of which almost all are oncogenes (n = 13/15) and TSGs (n = 10/11; $p < 0.0005$), respectively. Thus, oncogenes and TSGs of specific human cancers are expressed to relatively high and low levels, respectively, in the Prom1^{+} stem cells that generate these cancers in mice. Therefore, we reasoned that LRD scores might predict which of the 539 unclassified genes are oncogenes or TSGs.

Fifteen percent (n = 85/539) of the unclassified genes had an LRD >3 and are therefore predicted to be oncogenes. Interestingly, these were highly enriched for regulators of immune activation (GO:0006955, false discovery rate [FDR] = 2.6×10^{-4}), including *CD274* (*PDL1*) and *CTLA4* that suppress T cell function and are emerging as a new class of targets of cancer immunotherapy (Pardoll, 2012). While the functional consequences of these mutations remain unclear, PDL1 was recently demonstrated to drive T-ALL malignancies (Casey et al., 2016); therefore, we propose these aberrations enable early transforming stem cells to escape immunosurveillance. A further 6% (n = 34/539) of unclassified genes had an LRD <−3 and are therefore predicted to be TSGs (Figure 6C). These included *NEFH* that is hypermethylated in breast cancer (Calmon et al., 2015) and *JARID2*, a component of the Polycomb Repressor 2 Complex that negatively regulates hematopoietic stem cells (Kinkel et al., 2015).

DISCUSSION

Vigorous debate has surrounded two apparently opposing explanations of why cancers are distributed unevenly among organs. One idea proposes that extrinsic carcinogens drive this bias; the other is that intrinsic factors e.g., stem cell proliferation,

Figure 5. Stem Cell Activity and Tumor Susceptibility Are Functionally Related in Prom1^{+} Liver Cells

(A) Concurrent β-galactosidase and direct GFP fluorescence of the same section of liver taken from an adult *Prom1*$^{C\text{-}L}$;*Rosa*^{ZsG} mouse that underwent tamoxifen-recombination as a neonate. Arrows identify β-gal^{+}/GFP^{+} cells and the percentage of these cells in four separate livers is shown below. Scale bar, 50 μm.

(B) Prom1^{+} cell generative capacity in adult mouse livers harboring two different lineage tracing alleles and damaged by DDC treatment or partial hepatectomy. Scale bars, 50 μm.

(C) Unsupervised hierarchical clustering of Prom1^{+} cell transcriptomes isolated normal newborn (NB^{NT}) and adult (AD^{NT}) livers as well as adult livers treated with DDC (AD^{DDC}).

(D) AGDEX comparison of NB^{NT} and AD^{DDC} Prom1^{+} cell transcriptomes using the AD^{NT} Prom1^{+} cell transcriptome as a common comparator.

(E) Left: survival curves of adult control and DDC-treated *Prom1*$^{C\text{-}L}$;*Rosa*^{ZsG} mice carrying the indicated alleles. p value, difference in survival. Right: anatomical heatmaps of organ tumor incidence. Below, ratios of tumors in neonatal and adult liver. F, Fisher's test of the difference; CMH, Cochran-Mantel-Haenszel test of the difference.

See also Figure S1 and Table S2.

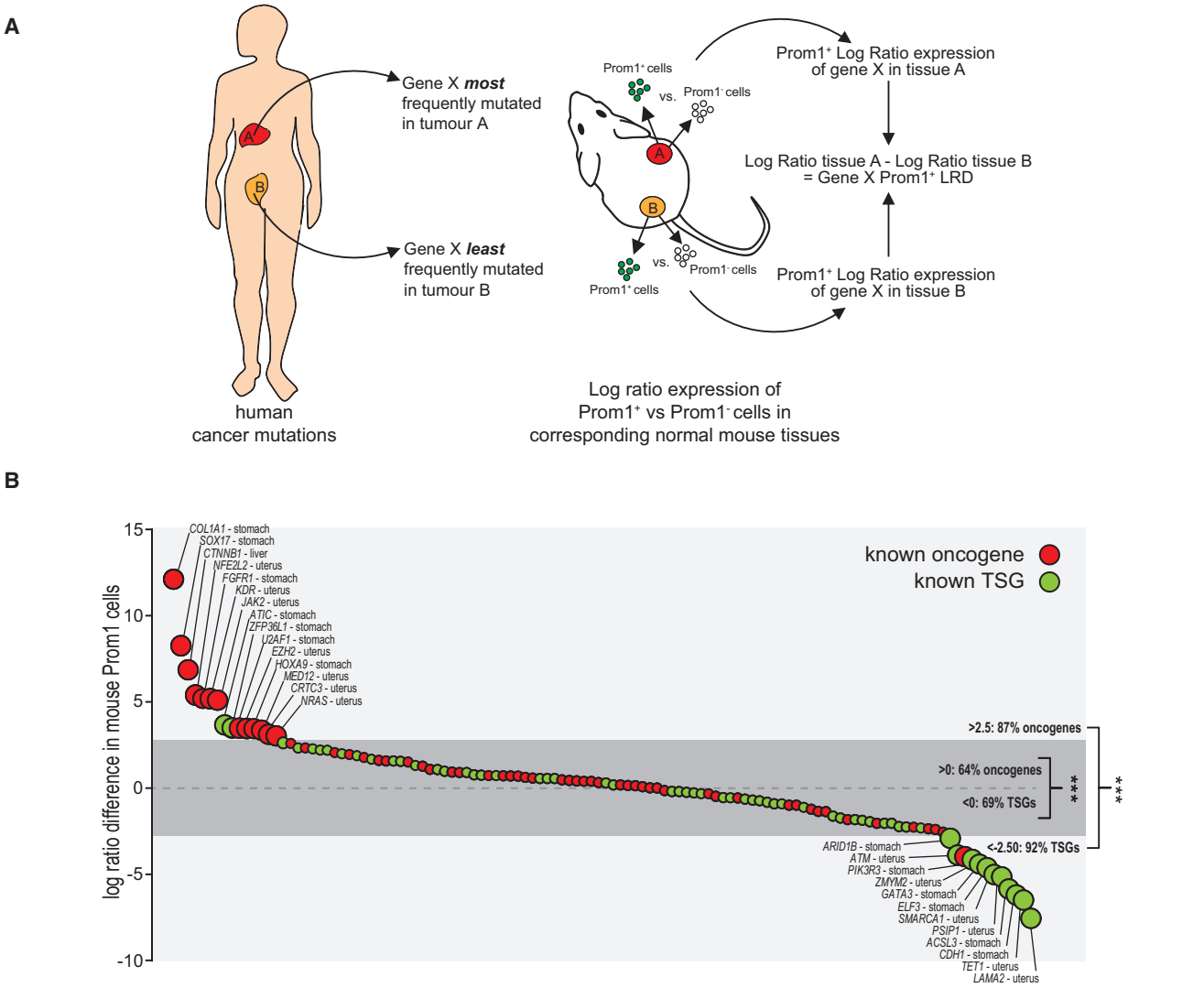

(legend on next page)

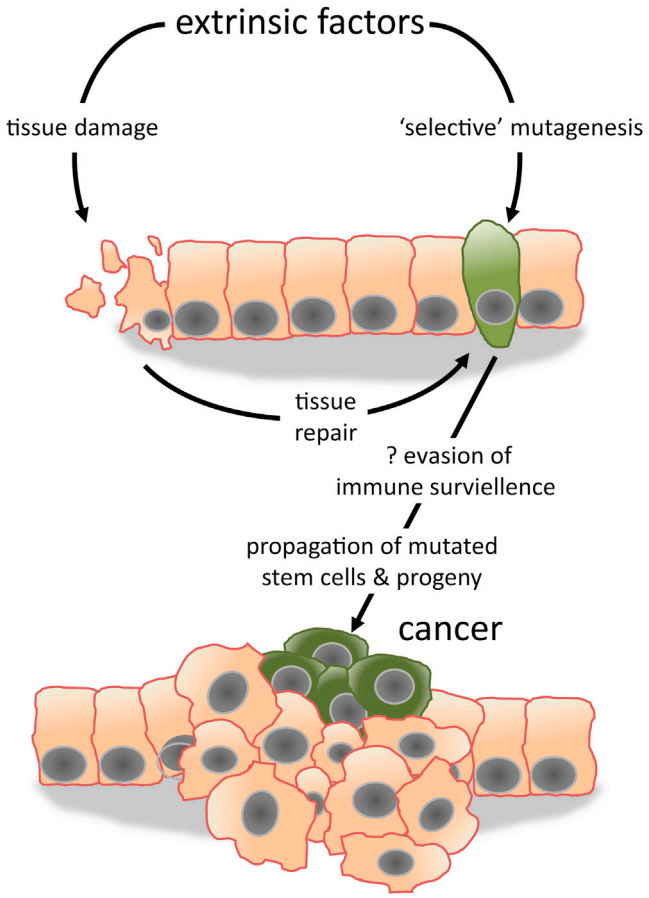

Figure 7. Proposed Model for the Role of Cell Intrinsic and Extrinsic Factors in Determining Organ Cancer Risk

We propose that extrinsic factors converge specifically on stem cells to induce mutations and/or tissue damage that provokes proliferative repair. Tissue-specific susceptibility of stem cells to induced mutations and their intrinsic, or damage-induced proliferative capacity, create a "perfect storm" that ultimately determines organ cancer risk. The high expression of immune regulators by stem cells might enable early transforming cells to escape immunosurveillance.

See also STAR Methods.

can independently dictate cancer risk. However, because intrinsic and extrinsic factors are likely to cooperate, correlational analyses of human epidemiological data cannot assess their relative importance. Here, using a series of conditional oncogene and TSG alleles, we selectively introduced mutations into well-characterized stem and non-stem cell populations across organs in mice, essentially circumventing the need for mutagenic extrinsic factors and therefore testing the role of intrinsic factors in cancer risk. We show that the risk of an organ developing cancer is significantly associated with the life-long generative capacity of its mutated cells. This relationship held true in the presence of multiple genotypes and regardless of developmental stage, strongly supporting the notion that stem cells can dictate cancer risk among organs.

However, our data by no means undermine the importance of extrinsic factors for cancer risk. The introduction of mutations into Prom1$^+$ cells of the normal adult liver was insufficient to induce tumors; only when extrinsic damage induced these cells to proliferate were they competent to transform. Tissue damage and inflammation are well recognized determinants of cancer risk across a variety of organs, but most studies have suggested that this damage is either mutagenic e.g., through production of reactive oxygen species, or promotes the survival and proliferation of transformed cells (Coussens and Werb, 2002; Shalapour and Karin, 2015). Our data suggest that the "carcinogenic" properties of some extrinsic factors might relate solely to their induction of local tissue damage and activation of stem cell repair, thereby creating an expanded population of cells that are competent for transformation. In this model, organ cancer risk could be determined by a critical combination of factors: the intrinsic proliferative capacity of the resident stem cell population, the presence of local tissue damage that expands the size of this population, the susceptibility of this population to be transformed by acquired mutations, and perhaps the presence of a stem cell transcriptome that allows the evasion of immunosurveillance. This model also allows for the scenario in which damage induces the acquisition of stem cell properties by relatively plastic cell populations (Figure 7).

As well as determining the distribution of cancer among different organs, stem cells may also dictate temporal patterns of cancer risk within the same organ. We show on average that neonatal Prom1$^+$ cells are far less likely to undergo transformation than those in adults with equivalent generative capacities, suggesting neonatal stem cells are intrinsically resistant to transformation. If this biology holds true in humans, then it may explain why cancer rates are many-fold lower in children than adults, despite the fact that childhood cancers accrue significant numbers of non-synonymous mutations, and organ growth rates peak in childhood (Jones and Baker, 2014; WHO Multicentre Growth Reference Study Group, 2006). Temporal stem cell context might also dictate cancer type. For example, in our models, hepatoblastoma—a childhood-specific liver tumor—was induced only by aberrant Notch signaling in neonatal Prom1$^+$ liver stem cells. Activation of NOTCH signaling is a recognized feature of hepatoblastoma (López-Terrada et al., 2009).

Our data also suggest that transforming stem cells may do more than merely propagate mutations. Recurrently mutated

Figure 6. Cross-Species Comparison of Gene Mutation and Expression in Human Cancers and Tissue-Matched Prom1$^+$ Stem Cells Predicts Oncogene and TSG Function

(A) Overall approach taken to calculate the log-ratio difference (LRD) of each gene (see STAR Methods).

(B) LRDs of known oncogenes and TSGs in liver, stomach, prostate, and uterus. Dark gray zone, LRD −3 to +3.

(C) Predicted function of recurrently mutated genes in liver, stomach, prostate, and uterine cancers based on LRD −3 to +3. Note preponderance of immune regulators in predicted oncogenes.

See also STAR Methods.

human cancer genes that were expressed at relatively high levels in Prom1$^+$ stem cells were strikingly enriched for immune regulators, including Ctla4 and Cd274 (Pdl1) that are targets of effective immune checkpoint inhibitors in cancer (Melero et al., 2015). We propose that the expression of these genes enables transforming stem cells to escape immunosurveillance at the earliest stages of tumorigenesis. Further work will be required to determine the precise characteristics that render stem cells vulnerable to transformation; but these may include the tolerance of oncogenic insults that might otherwise induce cellular apoptosis or senescence.

In addition to providing important insights into cancer origins, we identify a number of new Prom1$^+$ stem cell populations in several mouse organs including the neonatal and damaged adult liver, stomach, uterus, and prostate. At least two populations of well-characterized stem cells are known to exist in the adult mouse liver: peri-central vein Axin2$^+$ hepatocytes that constantly regenerate undamaged liver (Wang et al., 2015) and damage-induced, peri-portal Lgr5$^+$ cells that repair the liver (Huch et al., 2013). Here, we identify a previously unrecognized population of neonatal Prom1$^+$ liver stem cells with remarkable generative capacity that essentially produce most if not all cells of the early postnatal and juvenile liver. These cells are located within or adjacent to the Krt19$^+$ bile duct epithelium and are therefore distinct from peri-central vein Axin2$^+$ stem cells that perform a similar function in the adult liver. Neonatal Prom1$^+$ liver cells also express low levels of Lgr5$^+$, as do their damage-responsive Prom1$^+$ progeny in adults, suggesting these cells are different from previously described Lgr5$^+$ liver stem cells. Similar to the liver, the number and location of Prom1$^+$ cells in other organs differed little between neonates and adults (e.g., lung). Therefore, it will be important to determine if neonatal Prom1$^+$ cells in these organs also give rise to quiescent but reparative and tumorigenic Prom1$^+$ cells in adults.

The various cancer models described here display remarkable histological and transcriptomic similarities to the corresponding human diseases and should therefore add significantly to the existing armamentarium of mouse cancer models available for biology and therapeutic studies. A number of organs in our mice generated few or no cancers (e.g., salivary gland, pancreas, and kidney) even though these tissues contained large numbers of Prom1$^+$ cells and can be transformed by the same oncogenes and TSGs used in our study (Clark et al., 2011; Hingorani et al., 2005; Raimondi et al., 2006). Our hypothesis proposes that these tissues did not develop cancer because they lacked Prom1$^+$ stem cells; however, because many of our mice developed multiple tumors, it is possible that cancers with shorter latencies arose and killed mice before they could develop salivary gland, pancreatic, or kidney tumors. Although feasible, we believe this is unlikely because the median survival of mice harboring activated *Kras* and *Ctnnb1* alleles in our study was equal to or greater than the published latency of salivary gland, pancreatic, and kidney cancers in mouse models driven by these alleles.

In summary, our data provide direct experimental evidence that the mutation of stem cells is an important determinant of cancer risk. We propose that extrinsic factors converge on these cell populations, inducing mutations and/or proliferation that together create the conditions necessary to drive tumorigenesis.

STAR★METHODS

Detailed methods are provided in the online version of this paper and include the following:

- KEY RESOURCES TABLE
- CONTACT FOR REAGENT AND RESOURCE SHARING
- EXPERIMENTAL MODEL AND SUBJECT DETAILS
  - Mice
- METHOD DETAILS
  - Mouse and Tissue Handling
  - Immunohistochemistry and Immunofluorescence
  - Orchidectomy and Testosterone Implantation
  - Partial Hepatectomy
  - Ultrasound Scans of Prostate
  - Two-Photon Laser-Scanning Microscopy
  - Single Cells Isolation from Mouse Organs
- QUANTIFICATION AND STATISTICAL ANALYSIS
  - Quantification of Prom1$^+$ Cell Characteristics
  - Gene Expression Microarrays, Agreement of Differential Expression, and Gene Set Enrichment Analyses
  - Statistical Modeling
- DATA AND SOFTWARE AVAILABILITY
  - Data Resources

SUPPLEMENTAL INFORMATION

Supplemental Information includes three figures and four tables and can be found with this article online at http://dx.doi.org/10.1016/j.cell.2016.07.045.

A video abstract is available at http://dx.doi.org/10.1016/j.cell.2016.07.045#mmc5.

AUTHOR CONTRIBUTIONS

L.Z. conducted the great majority of experiments. H.P., D.F., L.S., M.W., S.B.P., G.N., and S.U. conducted experiments. D.L.-T. and D.W.E. provided pathology expertise. K.W. provided expertise on liver biology. C.L.G. and L.S. performed AGDEX analyses with guidance from S.B.P. As co-corresponding authors, A.O.-T. and R.J.G. are responsible for all data, figures, and text. As lead author, R.J.G. conceived and oversaw the entire research project and serves as the primary contact for all communication and reagent and resource sharing.

ACKNOWLEDGMENTS

This work was supported by grants from the NIH (P01CA96832, R01, and P30CA021765 to R.J.G.), the American Lebanese Syrian Associated Charities, and Cancer Research UK. We are grateful to the staff of the Hartwell Center for Bioinformatics and Biotechnology, the Cell and Tissue Imaging Shared Resource, and the ARC at St. Jude Children's Research Hospital for technical assistance.

Received: February 6, 2016
Revised: May 12, 2016
Accepted: July 26, 2016
Published: August 25, 2016

REFERENCES

Arndt, K., Grinenko, T., Mende, N., Reichert, D., Portz, M., Ripich, T., Carmeliet, P., Corbeil, D., and Waskow, C. (2013). CD133 is a modifier of hematopoietic progenitor frequencies but is dispensable for the maintenance of mouse hematopoietic stem cells. Proc. Natl. Acad. Sci. USA *110*, 5582–5587.

Ashford, N.A., Bauman, P., Brown, H.S., Clapp, R.W., Finkel, A.M., Gee, D., Hattis, D.B., Martuzzi, M., Sasco, A.J., and Sass, J.B. (2015). Cancer risk: role of environment. Science *347*, 727.

Barker, N., Huch, M., Kujala, P., van de Wetering, M., Snippert, H.J., van Es, J.H., Sato, T., Stange, D.E., Begthel, H., van den Born, M., et al. (2010). Lgr5(+ve) stem cells drive self-renewal in the stomach and build long-lived gastric units in vitro. Cell Stem Cell *6*, 25–36.

Bennoun, M., Rissel, M., Engelhardt, N., Guillouzo, A., Briand, P., and Weber-Benarous, A. (1993). Oval cell proliferation in early stages of hepatocarcinogenesis in simian virus 40 large T transgenic mice. Am. J. Pathol. *143*, 1326–1336.

Bienz, M., and Clevers, H. (2000). Linking colorectal cancer to Wnt signaling. Cell *103*, 311–320.

Block, T.M., Mehta, A.S., Fimmel, C.J., and Jordan, R. (2003). Molecular viral oncology of hepatocellular carcinoma. Oncogene *22*, 5093–5107.

Boyce, S., and Harrison, D. (2008). A detailed methodology of partial hepatectomy in the mouse. Lab Anim. (NY) *37*, 529–532.

Calmon, M.F., Jeschke, J., Zhang, W., Dhir, M., Siebenkäs, C., Herrera, A., Tsai, H.-C., O'Hagan, H.M., Pappou, E.P., Hooker, C.M., et al. (2015). Epigenetic silencing of neurofilament genes promotes an aggressive phenotype in breast cancer. Epigenetics *10*, 622–632.

Casey, S.C., Tong, L., Li, Y., Do, R., Walz, S., Fitzgerald, K.N., Gouw, A.M., Baylot, V., Gütgemann, I., Eilers, M., and Felsher, D.W. (2016). MYC regulates the antitumor immune response through CD47 and PD-L1. Science *352*, 227–231.

Clark, P.E., Polosukhina, D., Love, H., Correa, H., Coffin, C., Perlman, E.J., de Caestecker, M., Moses, H.L., and Zent, R. (2011). β-Catenin and K-RAS synergize to form primitive renal epithelial tumors with features of epithelial Wilms' tumors. Am. J. Pathol. *179*, 3045–3055.

Coussens, L.M., and Werb, Z. (2002). Inflammation and cancer. Nature *420*, 860–867.

Danaei, G., Vander Hoorn, S., Lopez, A.D., Murray, C.J., and Ezzati, M.; Comparative Risk Assessment collaborating group (Cancers) (2005). Causes of cancer in the world: comparative risk assessment of nine behavioural and environmental risk factors. Lancet *366*, 1784–1793.

Engreitz, J.M., Daigle, B.J., Jr., Marshall, J.J., and Altman, R.B. (2010). Independent component analysis: mining microarray data for fundamental human gene expression modules. J. Biomed. Inform. *43*, 932–944.

Fournier, D.A., Skaug, H.J., Ancheta, J., Ianelli, J., Magnusson, A., Maunder, M., Nielsen, A., and Sibert, J. (2012). AD Model Builder: using automatic differentiation for statistical inference of highly parameterized complex nonlinear models. Optim. Methods Softw. *27*, 233–249.

Futreal, P.A., Coin, L., Marshall, M., Down, T., Hubbard, T., Wooster, R., Rahman, N., and Stratton, M.R. (2004). A census of human cancer genes. Nat. Rev. Cancer *4*, 177–183.

Gotay, C., Dummer, T., and Spinelli, J. (2015). Cancer risk: prevention is crucial. Science *347*, 728.

Hand, N.J., Master, Z.R., Le Lay, J., and Friedman, J.R. (2009). Hepatic function is preserved in the absence of mature microRNAs. Hepatology *49*, 618–626.

Harada, N., Tamai, Y., Ishikawa, T., Sauer, B., Takaku, K., Oshima, M., and Taketo, M.M. (1999). Intestinal polyposis in mice with a dominant stable mutation of the beta-catenin gene. EMBO J. *18*, 5931–5942.

Hingorani, S.R., Wang, L., Multani, A.S., Combs, C., Deramaudt, T.B., Hruban, R.H., Rustgi, A.K., Chang, S., and Tuveson, D.A. (2005). Trp53R172H and KrasG12D cooperate to promote chromosomal instability and widely metastatic pancreatic ductal adenocarcinoma in mice. Cancer Cell *7*, 469–483.

Houghton, J., Stoicov, C., Nomura, S., Rogers, A.B., Carlson, J., Li, H., Cai, X., Fox, J.G., Goldenring, J.R., and Wang, T.C. (2004). Gastric cancer originating from bone marrow-derived cells. Science *306*, 1568–1571.

Howlader, N., Noone, A.M., Krapcho, M., Neyman, N., Aminou, R., Altekruse, S.F., Kosary, C.L., Ruhl, J., Tatalovich, Z., Cho, H., et al. (2012). SEER Cancer Statistics Review, 1975-2009 (National Cancer Institute Bethesda).

Huch, M., Dorrell, C., Boj, S.F., van Es, J.H., Li, V.S.W., van de Wetering, M., Sato, T., Hamer, K., Sasaki, N., Finegold, M.J., et al. (2013). In vitro expansion of single Lgr5+ liver stem cells induced by Wnt-driven regeneration. Nature *494*, 247–250.

Johnson, R.A., Wright, K.D., Poppleton, H., Mohankumar, K.M., Finkelstein, D., Pounds, S.B., Rand, V., Leary, S.E., White, E., Eden, C., et al. (2010). Cross-species genomics matches driver mutations and cell compartments to model ependymoma. Nature *466*, 632–636.

Jones, C., and Baker, S.J. (2014). Unique genetic and epigenetic mechanisms driving paediatric diffuse high-grade glioma. Nat. Rev. Cancer *14*, 651–661.

Kinkel, S.A., Galeev, R., Flensburg, C., Keniry, A., Breslin, K., Gilan, O., Lee, S., Liu, J., Chen, K., Gearing, L.J., et al. (2015). Jarid2 regulates hematopoietic stem cell function by acting with polycomb repressive complex 2. Blood *125*, 1890–1900.

Kong, D., Suzuki, A., Zou, T.T., Sakurada, A., Kemp, L.W., Wakatsuki, S., Yokoyama, T., Yamakawa, H., Furukawa, T., Sato, M., et al. (1997). PTEN1 is frequently mutated in primary endometrial carcinomas. Nat. Genet. *17*, 143–144.

Lee, A., Kessler, J.D., Read, T.-A., Kaiser, C., Corbeil, D., Huttner, W.B., Johnson, J.E., and Wechsler-Reya, R.J. (2005). Isolation of neural stem cells from the postnatal cerebellum. Nat. Neurosci. *8*, 723–729.

López-Terrada, D., Gunaratne, P.H., Adesina, A.M., Pulliam, J., Hoang, D.M., Nguyen, Y., Mistretta, T.A., Margolin, J., and Finegold, M.J. (2009). Histologic subtypes of hepatoblastoma are characterized by differential canonical Wnt and Notch pathway activation in DLK+ precursors. Hum. Pathol. *40*, 783–794.

Masuda, H., Maruyama, T., Hiratsu, E., Yamane, J., Iwanami, A., Nagashima, T., Ono, M., Miyoshi, H., Okano, H.J., Ito, M., et al. (2007). Noninvasive and real-time assessment of reconstructed functional human endometrium in NOD/SCID/gamma c(null) immunodeficient mice. Proc. Natl. Acad. Sci. USA *104*, 1925–1930.

McCulloch, C.E., Searle, S.R., and Neuhaus, J.M. (2008). Generalized, Linear and Mixed Models, Second Edition (Wiley).

Melero, I., Berman, D.M., Aznar, M.A., Korman, A.J., Pérez Gracia, J.L., and Haanen, J. (2015). Evolving synergistic combinations of targeted immunotherapies to combat cancer. Nat. Rev. Cancer *15*, 457–472.

Michalopoulos, G.K., and DeFrances, M.C. (1997). Liver regeneration. Science *276*, 60–66.

O'Brien, C.A., Pollett, A., Gallinger, S., and Dick, J.E. (2007). A human colon cancer cell capable of initiating tumour growth in immunodeficient mice. Nature *445*, 106–110.

O'Callaghan, M. (2015). Cancer risk: accuracy of literature. Science *347*, 729.

Pardoll, D.M. (2012). The blockade of immune checkpoints in cancer immunotherapy. Nat. Rev. Cancer *12*, 252–264.

Pikarsky, E., Porat, R.M., Stein, I., Abramovitch, R., Amit, S., Kasem, S., Gutkovich-Pyest, E., Urieli-Shoval, S., Galun, E., and Ben-Neriah, Y. (2004). NF-kappaB functions as a tumour promoter in inflammation-associated cancer. Nature *431*, 461–466.

Potter, J.D., and Prentice, R.L. (2015). Cancer risk: tumors excluded. Science *347*, 727.

Preisegger, K.H., Factor, V.M., Fuchsbichler, A., Stumptner, C., Denk, H., and Thorgeirsson, S.S. (1999). Atypical ductular proliferation and its inhibition by transforming growth factor beta1 in the 3,5-diethoxycarbonyl-1,4-dihydrocollidine mouse model for chronic alcoholic liver disease. Lab. Invest. *79*, 103–109.

Raimondi, A.R., Vitale-Cross, L., Amornphimoltham, P., Gutkind, J.S., and Molinolo, A. (2006). Rapid development of salivary gland carcinomas upon conditional expression of K-ras driven by the cytokeratin 5 promoter. Am. J. Pathol. *168*, 1654–1665.

Ricci-Vitiani, L., Lombardi, D.G., Pilozzi, E., Biffoni, M., Todaro, M., Peschle, C., and De Maria, R. (2007). Identification and expansion of human colon-cancer-initiating cells. Nature *445*, 111–115.

Risinger, J.I., Hayes, A.K., Berchuck, A., and Barrett, J.C. (1997). PTEN/MMAC1 mutations in endometrial cancers. Cancer Res. *57*, 4736–4738.

Shalapour, S., and Karin, M. (2015). Immunity, inflammation, and cancer: an eternal fight between good and evil. J. Clin. Invest. *125*, 3347–3355.

Shupe, T.D., Piscaglia, A.C., Oh, S.H., Gasbarrini, A., and Petersen, B.E. (2009). Isolation and characterization of hepatic stem cells, or "oval cells," from rat livers. Methods Mol. Biol. *482*, 387–405.

Singh, S.K., Hawkins, C., Clarke, I.D., Squire, J.A., Bayani, J., Hide, T., Henkelman, R.M., Cusimano, M.D., and Dirks, P.B. (2004). Identification of human brain tumour initiating cells. Nature *432*, 396–401.

Skaug, H., Fournier, D., Bolker, B., Magnusson, A., and Nielsen, A. (2014). Generalized linear mixed models using AD Model Builder (R package version 080).

Song, M., and Giovannucci, E.L. (2015). Cancer risk: many factors contribute. Science *347*, 728–729.

Tomasetti, C., and Vogelstein, B. (2015). Cancer etiology. Variation in cancer risk among tissues can be explained by the number of stem cell divisions. Science *347*, 78–81.

Wang, B., Zhao, L., Fish, M., Logan, C.Y., and Nusse, R. (2015). Self-renewing diploid Axin2(+) cells fuel homeostatic renewal of the liver. Nature *524*, 180–185.

WHO Multicentre Growth Reference Study Group (2006). WHO Child Growth Standards based on length/height, weight and age. Acta Paediatr. Suppl. *450*, 76–85.

Wild, C., Brennan, P., Plummer, M., Bray, F., Straif, K., and Zavadil, J. (2015). Cancer risk: role of chance overstated. Science *347*, 728.

Wu, S., Powers, S., Zhu, W., and Hannun, Y.A. (2016). Substantial contribution of extrinsic risk factors to cancer development. Nature *529*, 43–47.

Xin, L., Ide, H., Kim, Y., Dubey, P., and Witte, O.N. (2003). In vivo regeneration of murine prostate from dissociated cell populations of postnatal epithelia and urogenital sinus mesenchyme. Proc. Natl. Acad. Sci. USA *100* (*Suppl 1*), 11896–11903.

Yin, A.H., Miraglia, S., Zanjani, E.D., Almeida-Porada, G., Ogawa, M., Leary, A.G., Olweus, J., Kearney, J., and Buck, D.W. (1997). AC133, a novel marker for human hematopoietic stem and progenitor cells. Blood *90*, 5002–5012.

Zhu, L., Gibson, P., Currle, D.S., Tong, Y., Richardson, R.J., Bayazitov, I.T., Poppleton, H., Zakharenko, S., Ellison, D.W., and Gilbertson, R.J. (2009). Prominin 1 marks intestinal stem cells that are susceptible to neoplastic transformation. Nature *457*, 603–607.

STAR★METHODS

KEY RESOURCES TABLE

REAGENT or RESOURCE	SOURCE	IDENTIFIER
Antibodies		
Rabbit polyclonal anti-phospho-histone H3 (Ser10)	Millipore	Cat# 06-570; RRID: AB_310177
Rabbit polyclonal anti-androgen receptor	Sigma-Aldrich	Cat# A9853; RRID: AB_262132
Mouse monoclonal anti-p63	Santa Cruz	Cat# sc-8431; RRID: AB_628091
Rat monoclonal anti-A6	gift of N.V. Engelhardt, NIH, Bethesda, MD (Bennoun et al., 1993)	N/A
Rat monoclonal anti-Krt19	gift of J. Friedman, University of Pennsylvania, Philadelphia, PA (Hand et al., 2009)	N/A
Rabbit monoclonal anti-Krt19	Abcam	Cat# ab133496; RRID: AB_11155282
Mouse monoclonal anti-HNF4α	R&D System	Cat# PP-K9218-00; RRID: AB_2116902
Mouse monoclonal anti-β-catenin	BD Biosciences	Cat# 610153; RRID: AB_397554
Rabbit polyclonal anti-glutamine synthetase	Abcam	Cat# ab73593; RRID: AB_2247588
Rabbit polyclonal anti-Hes-1	Abcam	Cat# ab71559; RRID: AB_1209570
Rabbit polyclonal anti-Sall4	Abcam	Cat# ab29112; RRID: AB_777810
Mouse monoclonal anti-HepPar-1	Dako	Cat# M 7158; RRID: AB_2335689
Chemicals, Peptides, and Recombinant Proteins		
Tamoxifen	Sigma-Aldrich	Cat# T5648
Rhodamine-labeled DBA	Vector Laboratories	Cat# RL-1032; RRID: AB_2336396
rhodamine-labeled UEA I	Vector Laboratories	Cat# RL-1062; RRID: AB_2336769
GS II, Alexa Fluor 594 conjugate	Invitrogen	Cat# L-21416
Testosterone-propionate, 2.5 mg/pellet, 21-day release	Innovative Research of America	Cat# A-211
0.1% DDC rodent chow	Bio-Serv	Diet F4613
Critical Commercial Assays		
RNeasy Mini Kit	QIAGEN	Cat# 74104
PicoPure RNA extraction kit	Thermo Fisher	Cat# KIT0204
Dead Cell Removal Kit	Miltenyi Biotec	Cat# 130-090-101
MACS with anti-Prominin-1 MicroBeads	Miltenyi Biotec	Cat# 130-092-564
Deposited Data		
Raw and analyzed Affymetrix microarray data	This paper	GEO: GSE78076
Human cancer gene expression profiles	(Engreitz et al., 2010)	GEO: GSE64985
Recurrent mutations in human cancers	cBioPortal for Cancer Genomics	http://www.cbioportal.org
Experimental Models: Organisms/Strains		
Mouse: *Prom1*$^{C\text{-}L}$	Generated in our laboratory (Zhu et al., 2009)	RRID: IMSR_JAX:017743
Mouse: *Rosa*^{NICD1}	Jackson Laboratory	RRID: IMSR_JAX:008159
Mouse: *Rosa*^{ZsG}	Jackson Laboratory	RRID: IMSR_JAX:007906
Mouse: *Pten*^{flx}	Jackson Laboratory	RRID: IMSR_JAX:004597
Mouse: *Tp53*^{flx}	Jackson Laboratory	RRID: IMSR_JAX:008462
Mouse: *Cdkn2a*^{flx}	Jackson Laboratory	RRID: IMSR_JAX:023323
Mouse: *Kras*^{G12D}	NCI Mouse Repository	RRID: IMSR_NCIMR:01XJ6

(*Continued on next page*)

Continued

REAGENT or RESOURCE	SOURCE	IDENTIFIER
Mouse: *Ctnnb1*$^{flx(ex3)}$	from M. Taketo, Kyoto University, Japan (Harada et al., 1999)	N/A
Software and Algorithms		
AGDEX	(Johnson et al., 2010)	http://www.stjuderesearch.org/site/depts/biostats/agdex
GSEA	Broad Institute	http://software.broadinstitute.org/gsea
Non-parametric tests (Fisher's exact, Cochran-Mantel-Haenszel)	Minitab	Minitab 16.1.0
glmmADMB	(Fournier et al., 2012; Skaug et al., 2014)	http://glmmadmb.r-forge.r-project.org/

CONTACT FOR REAGENT AND RESOURCE SHARING

Further information and requests for reagents may be directed to, and will be fulfilled by the corresponding author Richard J. Gilbertson (richard.gilbertson@cruk.cam.ac.uk).

EXPERIMENTAL MODEL AND SUBJECT DETAILS

Mice

Mice were *Prom1*$^{C\text{-}L}$ (Zhu et al., 2009), *Rosa*^{NICD1}, *Rosa*^{ZsG}, *Pten*$^{flx/flx}$, *p53*$^{flx/flx}$, *Cdkn2a*$^{flx/flx}$ (Jackson Laboratory), *Kras*^{G12D} (NCI Mouse Repository) and *Ctnnb1*$^{flx(ex3)}$ (from M. Taketo). See "Key Resources Table" for details. All mice were maintained in a specific pathogen-free facility and all animal experiments were performed in accordance with protocols approved by the Institutional Animal Care and Use Committee of St. Jude Children's Research Hospital.

METHOD DETAILS

Mouse and Tissue Handling

Cre-recombination in mice was activated with 3mg tamoxifen (TMX)/40 g body weight at either neonatal (P1) or adult (typically P60) for two consecutive days by IP injection. Liver damage was induced in mice by partial hepatectomy or chow containing 0.1% DDC (Bio-Serv) commenced 3 days post TMX. Mouse prostate regeneration was induced by orchidectomy and serial testosterone implants. See below for detailed surgical procedures. Full-body necropsy was performed on moribund mice, or the indicated time point, whichever first. Tissue sections of all major mouse organs were subjected to direct GFP microscopy and β-galactosidase staining using 12 μm frozen sections or H&E and appropriate diagnostic immunostaining performed on 5 μm paraffin sections.

Immunohistochemistry and Immunofluorescence

For immunohistochemistry, tissues were fixed in 4% paraformaldehyde, paraffin embedded and sectioned at 5 μm. Antibodies for immunohistochemical staining (Figure 3A) include anti-β-catenin, anti-Glutamine Synthetase, anti-Hes-1, anti-Sall4, anti-Krt19 and anti-HepPar-1. For GFP microscopy and immunofluorescence, tissues were perfused and fixed in 2% paraformaldehyde, cryo-protected, frozen in OCT and sectioned at 12 μm. Antibodies for immunofluorescence staining (Figures S1 and S2) include anti-phospho Histone H3, anti-androgen receptor, anti-p63, anti-A6, anti-Krt19, and anti-HNF4α. Lectins for gastric mucosa staining (Figure S2) include rhodamine-labeled DBA, rhodamine-labeled UEA I, GS II, Alexa Fluor® 594 conjugate. See "Key Resources Table" for details.

Orchidectomy and Testosterone Implantation

Two-month-old male *Prom1*$^{C\text{-}L}$*; Rosa*^{ZsG} mice were castrated 3 days post tamoxifen treatment using standard techniques. Briefly, each mouse was anesthetized with 2%–3% isoflurane. A small incision was made rostral to the scrotal sac and gentle pressure applied to aid visualizing the testicles. The tunica albuginea was incised to separate and remove the testes from the scrotal ligament. Skin edges were adhered with tissue glue. Mice were allowed to rest for four weeks to ensure involution of the prostate prior to insertion of subcutaneous testosterone pellet implantation. Mice were anesthetized with 2%–3% isoflurane and a small skin incision made on the dorsal neck. A testosterone pellet (testosterone-propionate, 2.5 mg/pellet, 21-day release, Innovative Research of America) was inserted and placed 2 cm from the incision by a trochar (Innovative Research of America, Catalog No. MP-182). Tissue glue was used to close the skin edges. The procedure was repeated four times every eight weeks to induce repeated prostatic involution and regeneration that was monitored by ultrasound imaging.

Partial Hepatectomy

Partial hepatectomy in two month old *Prom1*^{CreERT2}*; Rosa*^{LacZ} mice was performed 3 days post tamoxifen treatment using standard techniques (Boyce and Harrison, 2008). Briefly, each mouse was anesthetized with 2%–3% isoflurane and a transverse abdominal incision made to expose the posterior section of the median lobe of the liver. The left and right median lobes of the liver were surgically removed. Sutures used to ligate the hepatic vessels and close the abdominal wall. Wound clips were used to close the skin.

Ultrasound Scans of Prostate

Mice were anesthetized with 2%–3% isofluorane in O_2 (2 l/min) and their hair removed from the lower ventral abdomen. Animals were then positioned ventrally and secured on the heated platform, allowing physiological monitoring throughout. Warmed Aquasonic 100 (Parker Laboratories) coupling gel was applied to the surface of the skin and target organs imaged (40 MHz) using a VEVO-770 High Resolution Ultrasound system (FujiFilm VisualSonics). Data were acquired with an in-plane resolution of 40 μm and a step-size of 0.102 mm and processed using the VEVO-770 software to provide volumetric information and rendering.

Two-Photon Laser-Scanning Microscopy

Two-photon laser-scanning microscopy was performed using an Ultima imaging system (Prairie Technologies), a Ti:sapphire Chameleon Ultra femtosecond-pulsed laser (930 nm) (Coherent), and a 20 × 0.95 NA water-immersion IR objective (Olympus). Stacks of images were reconstructed in 3D using Imaris software (Bitplane).

Single Cells Isolation from Mouse Organs

Liver was dissociated in situ with Liberase-TM (0.1 U/ml; Roche) in Krebs' Ringer with glucose (3.6 g/L) and calcium (1 mM) as described (Shupe et al., 2009).

Prostates were dissociated with 800 μg/ml collagenase type I (Worthington) and 100 μg/ml DNase I (Roche) in DMEM (Lonza) supplemented with 2mM L-glutamine (Invitrogen), 100 U/ml penicillin, 100 μg/ml streptomycin (Invitrogen) and 10% fetal bovine serum (Atlanta Biologicals) at 37°C for 90 min as described (Xin et al., 2003).

Stomachs were removed from 20 mice, opened, and washed extensively in PBS. The mucosa was scraped off the pyloric region and digested for 60 min at 37° in 0.1% Pronase (Roche) and 100 μg/ml DNase I (Roche) in PBS containing 2% BSA and 1mM EDTA as described (Houghton et al., 2004).

Uteruses were dissociated with 0.2% collagenase type I (Worthington) and 100 μg/ml DNase I (Roche) in DMEM (Lonza) supplemented with 2 mM L-glutamine (Invitrogen), 100 U/ml penicillin, 100 μg/ml streptomycin (Invitrogen) and 10% fetal bovine serum (Atlanta Biologicals) at 37°C for 90 min as described (Masuda et al., 2007).

Salivary glands and kidneys were digested with 20 U/ml Papain (Sigma) and 100 μg/ml DNase I (Roche) in DMEM (Lonza) supplemented with 2 mM L-glutamine (Invitrogen), 100 U/ml penicillin, 100 μg/ml streptomycin (Invitrogen) and 10% fetal bovine serum (Atlanta Biologicals) at 37°C for 30-60 min.

QUANTIFICATION AND STATISTICAL ANALYSIS

Quantification of Prom1$^+$ cell population size, proliferative capacity, and generative capacity was performed on multiple tissue sections gathered from 10 separate mice.

Where appropriate, Figure Legends define the statistical test and associated parameters used to analyse data displayed in the corresponding Figure. Data are judged to be statistically significant when $p < 0.05$ in applied statistical analysis. In Figures 1 and 6, asterisks denote statistical significance (*, $p < 0.05$; **, $p < 0.01$; ***, $p < 0.001$).

Quantification of Prom1$^+$ Cell Characteristics

Prom1$^+$ cell population size, Prom1$^+$ cell proliferative capacity, Prom1$^+$ cell generative capacity and global organ proliferative capacity were quantified using frozen tissue sections of the appropriate organs taken from *Prom1*$^{C\text{-}L/+}$*; Rosa*^{ZsG} mice that had undergone tamoxifen recombination as described. For each analysis, 12 μm frozen sections were prepared from three separate and representative areas of each organ from a minimum of 10 individual *Prom1*$^{C\text{-}L/+}$*; Rosa*^{ZsG} mice at each time point ('basal' and 'aged' organs, 30 sections each per organ per time point). For assessments of Prom1$^+$ cell population size, sections were subjected to β-galactosidase staining and counterstained with nuclear fast red (Vector Laboratories). The Prom1$^+$ cell population size was then calculated as the average percentage of β-galactosidase$^+$ nuclei per total nuclei in each organ by counting a minimum of ~15,000 nuclei across the 30 sections of each organ. Note, because different organs display significantly different macro- and microscopic morphologies, including wide variations in cellular density and nuclear size, we did not employ automated imaging software to count cells but performed all counts manually.

We took a very similar approach to calculate Prom1$^+$ cell proliferative capacity, although frozen sections were subjected to pH3 and GFP co-immunofluorescence as described above and counterstained with DAPI (Vector Laboratories). The average percentage of GFP$^+$/pH3$^+$ double-positive nuclei per total GFP$^+$ cells was then calculated for each organ by counting a minimum of 15,000 nuclei across the 30 sections of each organ. To assess the global proliferative capacity of each organ we similarly calculated the average percentage of pH3$^+$ nuclei per total nuclei in each organ. Finally, to calculate the Prom1$^+$ cell generative capacity, we calculated the

average percentage of GFP$^+$ nuclei in each 'basal' and 'aged' organ (one day post tamoxifen treatment, generated as described for the total GFP$^+$ cell count denominator in Prom1$^+$ cell proliferative capacity). Prom1$^+$ cell generative capacity was then calculated by subtracting the average percentage of GFP$^+$ nuclei in 'basal' organs from the average percentage of GFP$^+$ nuclei in the corresponding 'aged' organs.

Gene Expression Microarrays, Agreement of Differential Expression, and Gene Set Enrichment Analyses

Total RNA of mouse normal and tumor tissues was extract using RNeasy Mini Kit (QIAGEN). Total RNA of Prom1$^+$ and Prom1$^-$ cells were extracted using PicoPure RNA extraction kit (Arcturus). mRNA expression profiles were generated using Affymetrix HT430 (mouse) array. Gene expression data were summarized and normalized using the RMA method as implemented in Partek Genomics Suite 6.6. The data were then imported into Spotfire Decision Site for Unsupervised Gene Hierarchical Clustering. Differences in gene expression between defined groups were calculated using a series of Welch t tests with a Bonferroni threshold at 0.05%. The agreement of differential expression (AGDEX) procedure was performed exactly as described previously (Johnson et al., 2010), and gene set enrichment analyses (GSEA) was performed using the online analytical resource from the Broad Institute (http://www.broadinstitute.org/gsea/index.jsp).

Statistical Modeling

We used Fisher's exact test or Cochran-Mantel-Haenszel (CMH) Test to capture possible associations between the likelihood of tumor formation and developmental stage across various genotypes within a tissue type. The former was used in tissue types where tumors formed in only 1 genotype for either the adult or the neonatal mice. In tissues where tumors were observed in multiple genotypes both for adult and neonatal mice, we used CMH test to assess this association. CMH is a generalization of the Fisher exact test and we used it to conditionally test the association of Tumor = Y/N versus adult/neonate in the presence of a third categorical variable, namely genotype. We used the same approach to also study the association between tumor formation and DDC use across genotypes. See STAR Methods for details.

DATA AND SOFTWARE AVAILABILITY

Data Resources

All microarray data have been deposited in GEO: GSE78076.

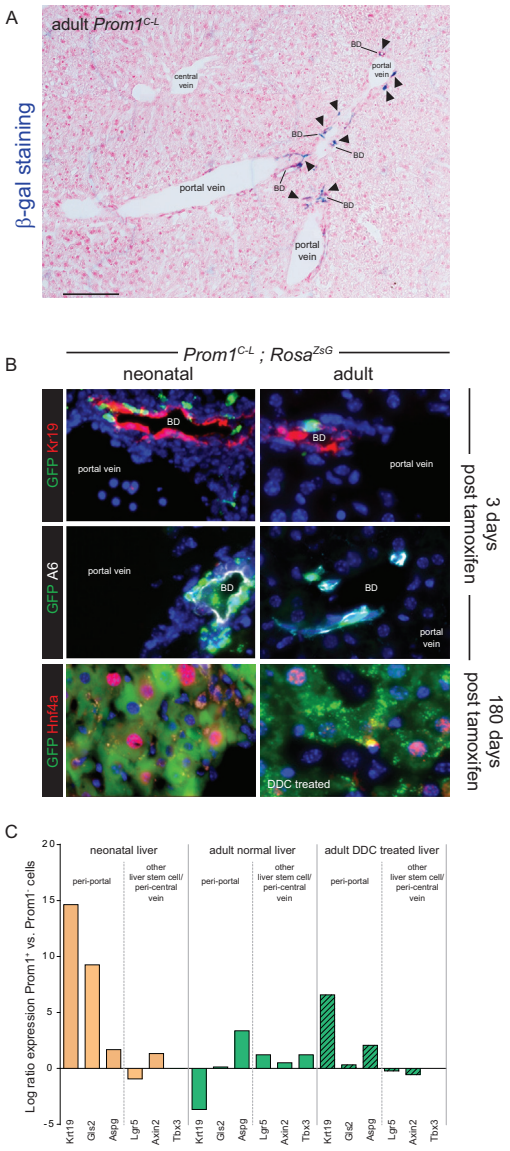

Figure S1. Prom1^{+} Cells Are Stem Cells in Normal Neonatal Liver and Damaged Adult Liver, Related to Figures 1 and 5

(A) β-galactosidase staining of Prom1C-L adult mouse liver identifies Prom1^{+} cells located around the bile ducts (bd).

(B) Co-immunofluorescence of GFP and: the bile duct epithelium marker Krt19; the liver progenitor cell marker A6; and the mature hepatocyte marker Hnf4α in neonatal (left) and adult (right) liver. The bottom right adult liver was treated with DDC following activation of the lineage tracing allele.

(C) Log-ratio of expression of established markers of peri-portal or other stem and peri-central liver stem cells in Prom1^{+} cells isolated from normal neonatal and adult livers (orange and green solid bars) and adult livers treated with DDC (green hashed bars).

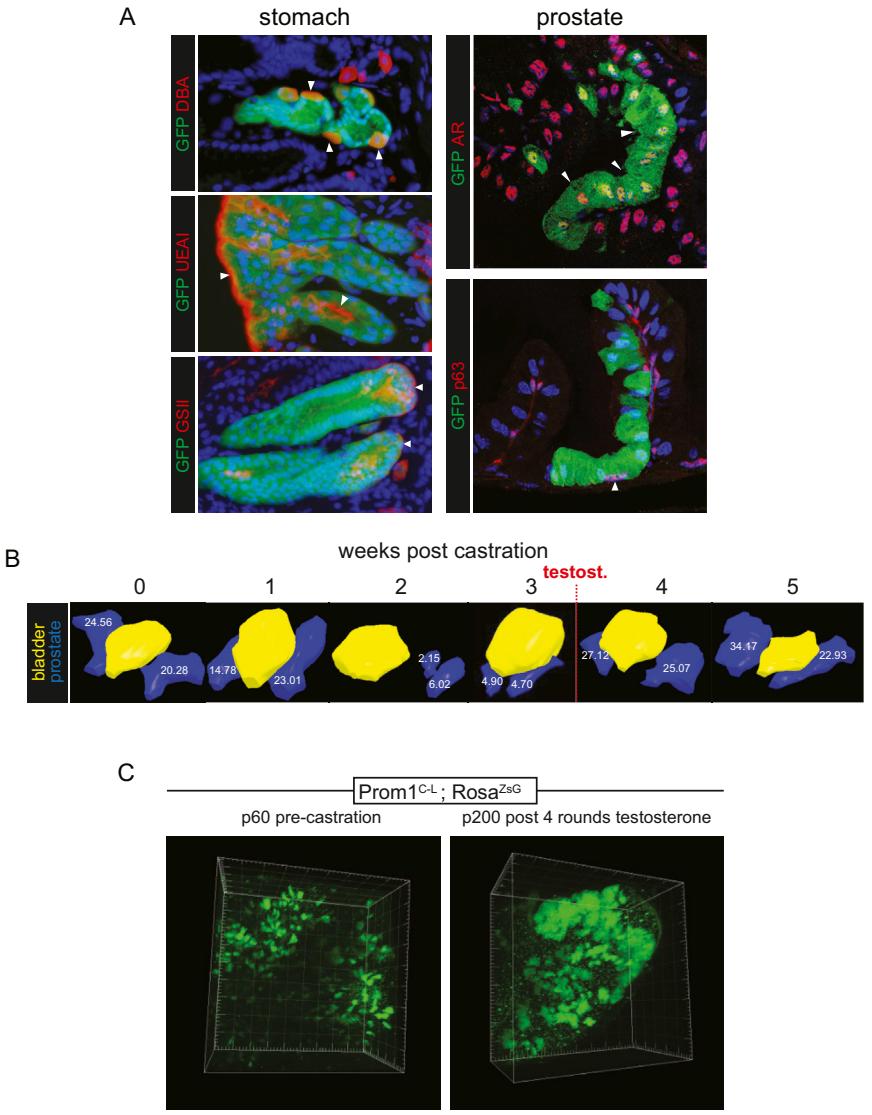

Figure S2. Prom1^{+} Cells Are Stem Cells in the Adult Stomach and Prostate, Related to Figure 1

(A) Adult *Prom1$^{C\text{-}L}$; Rosa^{ZsG}* mice were treated with tamoxifen and then 600 days later their stomach (left) and prostate (right) were removed and subjected to co-immunofluorescence of GFP and: left, markers of mature pit (UEAI^{+}), neck (GSII^{+}) and parietal (DBA^{+}) cells of the gastric epithelium; right, markers of basal (p63^{+}) and luminal (Androgen Receptor, AR^{+}) prostatic mucosal cells.

(B) Ultrasound scanning of prostatic involution and regeneration in castrated adult mice. Blue = prostate (numbers denote tissue volume), yellow = full bladder. Testost. = testosterone implantation.

(C) Two-photon laser scanning microscopic reconstructions of lineage traced prostate in castrated adult male *Prom1$^{C\text{-}L}$; Rosa^{ZsG}* mice treated in the same way as in B, showing progressive population of the prostatic mucosa with the GFP^{+} progeny of Prom1^{+} cells. Scale minor unit = 45 μm.

A

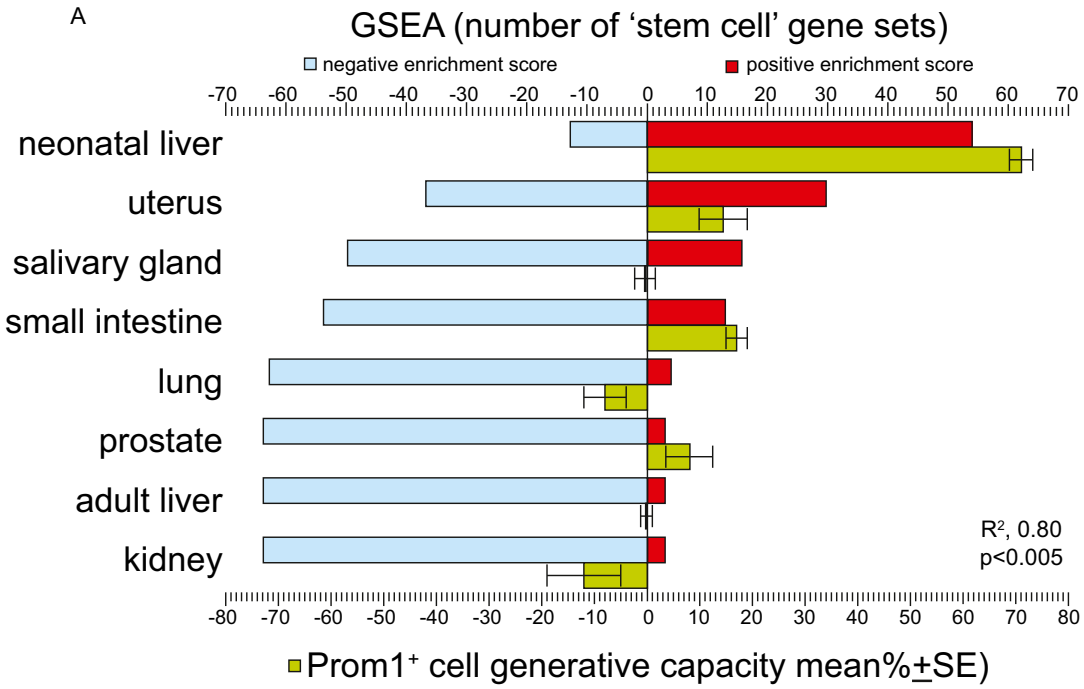

B

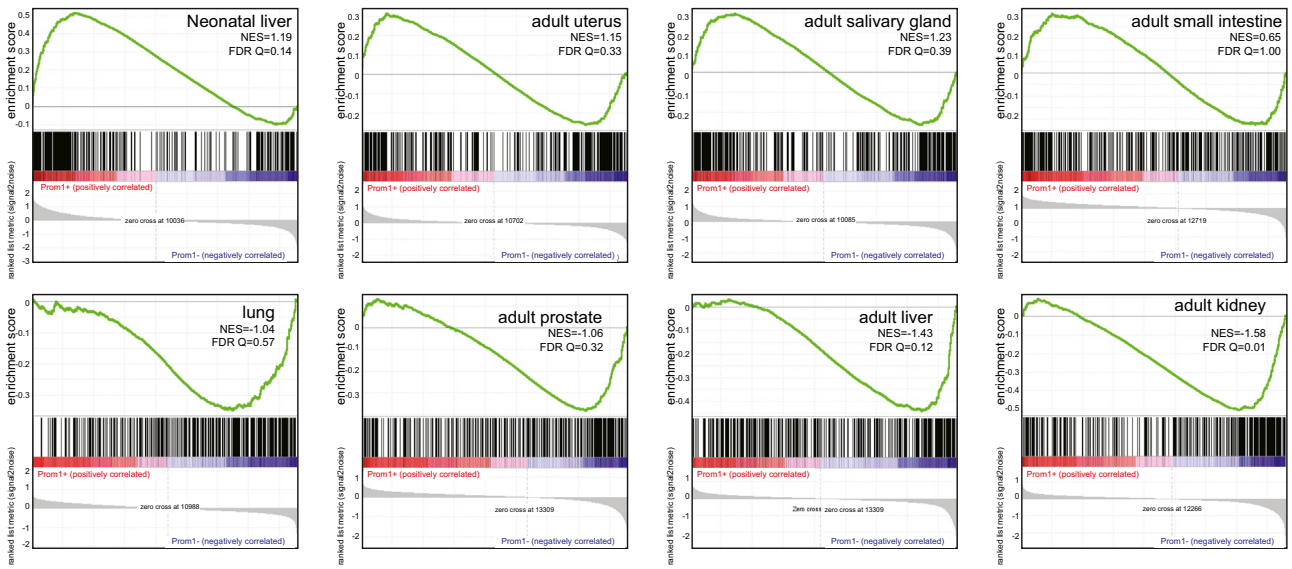

Figure S3. Prom1⁺ Cells with Extensive Generative Capacity Are Enriched for Established Stem Cell Transcriptomes, Related to Figure 1

(A) Graph depicting the number of 67 established stem cell signatures that displayed positive (Wild et al., 2015) or negative (blue) enrichment scores calculated by Gene Set Enrichment Analysis (GSEA) of Prom1⁺ cells isolated from the indicated tissues. The number of positively enriched signatures correlated closely with the generative capacity of the corresponding Prom1⁺ cell type.

(B) Relative enrichment of the published Lgr5⁺ stem cell signature in the indicated Prom1⁺ cells types.